Wireless Energy Harvesting Sensor Networks: Boolean-Poisson Modeling and Analysis

Ian Flint, Han-Bae Kong, *Member, IEEE*, Nicolas Privault,
Ping Wang, *Senior Member, IEEE* and Dusit Niyato, *Fellow, IEEE*

Abstract

Wireless radio frequency energy harvesting has been adopted in wireless networks as a method to supply energy to wireless nodes. In this paper, we analyze a wireless energy harvesting network based on a Boolean-Poisson model. This model assumes that energy sources are distributed according to a Poisson point process, and have disc-shaped coverage regions, with random radii. We introduce a distribution for the coverage radii which takes aggregated harvested power into account. The union of the coverage regions of the energy sources forms the energy harvesting zone. We derive the transmission success probability of single-hop networks characterized by the probability that two sensor nodes are located in the energy harvesting zone. Then, we analyze the performance of multi-hop networks in cases where the locations of the sensor nodes are either fixed or randomly distributed. Moreover, we consider a star-shaped topology which reflects the scenario wherein some sensor nodes simultaneously transmit data to a data collector. In this setting, we derive an approximation of the average throughput at the data collector. Numerical results validate the accuracy of our analysis in the single-hop and multi-hop networks and confirm the tightness of our approximation in the case of the star-shaped topology.

Index Terms

RF energy harvesting, Boolean-Poisson model, stochastic geometry, multi-hop networks.

I. Flint and N. Privault are with the School of Physical and Mathematical Sciences, Nanyang Technological University, Singapore 639798 (e-mail: iflint@ntu.edu.sg; nprivault@ntu.edu.sg).

H.-B. Kong, P. Wang and D. Niyato are with the School of Computer Engineering, Nanyang Technological University, Singapore 639798 (e-mail: hbkong@ntu.edu.sg; wangping@ntu.edu.sg; dniyato@ntu.edu.sg). H.-B. Kong is the corresponding author.

Part of this paper was presented at the IEEE Int. Conf. on Commun. (ICC), Kuala Lumpur, Malaysia, May 2016 [1].

I. Introduction

Recently, radio frequency (RF) energy harvesting techniques have been developed to let mobile and sensor nodes scavenge energy from radiated RF signals from ambient or dedicated RF sources [2]. Due to its advantages of powering energy-constrained devices and prolonging the lifetime of wireless networks, many researchers have studied energy harvesting methods in various wireless network scenarios, and implementations of RF energy harvesting techniques were presented in many experiments in [3]–[6].

One of the main issues in RF energy harvesting communication network is the modeling of the energy harvesting zone in the network. One can consider the coverage region of an RF energy source, i.e., an energy harvesting enabled area formed by the RF signals from the energy source. Then, the union of the coverage regions can be understood as the energy harvesting zone in the networks. In other words, energy constrained wireless nodes can harvest power to transmit or decode data if the nodes are located in the energy harvesting zone. In this sense, the probability that the nodes harvest energy is related not only to the distribution of the locations of the RF energy sources, but also to the characteristics of the coverage region.

In probability theory, the union of overlapping discs centered at random locations is known as the Boolean model. The Boolean model has been extensively studied, cf. [7] and [8] for a thorough overview, and the coverage properties of the model were investigated in [9]–[11]. In addition, the model has been used in different applications, see [7]. More specific examples are [12] for applications to image analysis and [13], [14] for applications to wireless networks. However, its application to wireless energy harvesting networks and the performance analysis of the networks have not been well studied in the literature.

A. Related Work and Motivations

In RF energy harvesting networks, there are mainly two types of RF energy sources, i.e., dedicated RF sources and ambient RF sources. In the networks with dedicated RF sources, energy harvesting nodes collect power from the RF signals sent by its dedicated RF energy transmitters [15]–[20]. In [15], simultaneous wireless information and power transfer (SWIPT) techniques for multiple-input multiple-output (MIMO) wireless broadcast systems were studied. The authors in [16] investigated a resource allocation algorithm in multiuser orthogonal frequency division multiplexing (OFDM) systems with SWIPT. Also, a power splitting technique for an

interference channel was proposed in [17]. References [18] and [19] introduced tradeoff between the information rate and the harvested energy for two-user and K-user interference channels, respectively. The performance of energy beamforming in wireless-powered communication networks was analyzed in [20]. Although energy harvesting nodes can efficiently scavenge power from the dedicated signals, deploying the dedicated RF sources leads to a high cost for the network.

In the networks with ambient RF sources, the energy harvesting nodes charge their battery from the RF signals radiated by nearby RF sources such as cellular base stations, TV radio towers, WiFi routers and mobile devices. Under the assumption that nodes harvest power from the aggregated RF signals from the energy sources which are distributed according to a Poisson point process (PPP), the performance of the energy harvesting networks was characterized in [21]–[25]. The study in [21] introduced a tradeoff among transmit power, density of base stations, and density of energy sources in an uplink cellular network. In [22], the authors derived the outage probability of a network overlaid with power beacons distributed according to a PPP. Alternatively, the authors in [23] investigated the transmission success probability in an RF energy harvesting multi-tier uplink cellular network by modeling the level of stored energy as a Markov chain. The ambient RF energy harvesting cognitive device-to-device communication was studied in [24]. In addition, the work in [25] proposed an approach for designing powered wireless networks and analyzed the performance of a hexagonal cellular network.

Unlike the works in [21]–[25], references [26]–[28] analyzed the performance of the ambient RF energy harvesting networks by introducing the energy harvesting zone. The authors in [26] characterized the transmission probability in wireless energy harvesting cognitive radio networks where transmitters in primary networks deliver RF energy to secondary transmitters located in the harvesting zone. Assuming that secondary transmitters scavenge power when they are located in the harvesting zone induced by both primary transmitters and Wi-Fi hotspots, the transmission probability was analyzed in [27]. Also, reference [28] developed a channel selection technique which maximizes the secondary throughput using an iterative algorithm.

However, previous works on networks with energy harvesting zone [26]–[28] only focused on the cognitive radio networks, and assumed that the radius of energy harvesting zone is fixed and deterministic. In other words, the previous works have not taken the features of the coverage regions into account when analyzing the networks. Furthermore, since the works in [26]–[28]

focused on a so-called typical node, it is intractable to extend the results to different networks where multiple nodes which communicate with each other simultaneously harvest energy. In this context, in this paper, we consider the Boolean-Poisson model which can reflect the characteristic of the coverage regions and consider the scenario where multiple nodes simultaneously scavenge energy.

B. Contributions and Organization

In this paper, we assume that the RF energy sources are distributed according to a homogeneous PPP, and the coverage region of an RF source is a disc of random radius. The Boolean-Poisson model then serves as a model for the energy harvesting zone of the networks. Based on this model, we analyze the performance of wireless energy harvesting networks where sensor nodes transmit or decode signals by utilizing the harvested power from the energy sources. The performance measures in terms of the energy harvesting probability, the transmission success probability and the average throughput are derived in various scenarios. The main contributions of this paper are summarized as follows:

- First, we provide the energy harvesting probability in single-hop networks that two sensor nodes are covered by the Boolean model with an arbitrary distribution of radii in Theorem 1. From Theorem 1, it is shown that the energy harvesting probability is a function of the distance between the nodes and the intensity of the RF energy sources. In addition, in (30), we provide a simplified expression for the energy harvesting probability for the case where the path loss exponent is equal to 2. Based on our results, we derive the transmission success probability which is the probability that the nodes successfully communicate with each other.
- Next, we extend the energy harvesting probability in Theorem 1 to the case of multiple nodes at aligned fixed locations. These nodes are part of a multi-hop link, and thus the important performance metric is the end-to-end transmission success probability. We derive an expression for the end-to-end transmission success probability which contains only a single integration.
- For the multi-hop networks, we also develop a tractable framework which takes randomly distributed multiple aligned nodes into account. More specifically, it is assumed in our framework that the nodes are distributed according to a general point process. We find that in

this setting the transmission success probability can be computed by numerical integration, cf. (58); furthermore, it can be computed efficiently employing the Quasi-Monte Carlo (QMC) technique which we introduce in Section VI-A.

- We also consider a network which we call "star-shaped topology". The network is composed of a data collector surrounded by n sensor nodes, and the sensor nodes transmit data to the data collector. In this setting, we introduce an approximation of the energy harvesting probability and then derive an approximation of the average throughput

From our numerical simulations, it is verified that our analytical results in the multi-hop networks accurately predict the performance and our analysis in the star-shaped topology approximates the actual average throughput very well.

This paper is organized as follows. The background on the Boolean-Poisson model and the network model are presented in Sections II and III, respectively. In Section IV, the energy harvesting and transmission success probabilities in single- and multi-hop networks are derived. Section V investigates the average throughput of the network with the star-shaped topology. In Section VI, we provide numerical results to validate our analysis. The conclusion of our work is made in Section VII.

II. The Boolean-Poisson Model

This section introduces the required background for the study of the Boolean-Poisson model which is also known as a Boolean model [8]. Please refer to [8] for further details.

The Boolean-Poisson model is driven by a PPP on $\mathbb{R}^d$ with intensity λ. Each point in the PPP is the center of a ball with random radius r, distributed according to a probability measure μ on $[0,\infty)$, independently from the other radii and from the PPP. More formally, we consider the probability space $(\Omega,\mathcal{F},\mathbb{P})$ on which we let Φ be a PPP supported on $\mathbb{R}^d\times[0,\infty)$, with intensity measure $(\lambda\ell)\times\mu$, where ℓ indicates the Lebesgue measure on $\mathbb{R}^d$ and $\cdot\times\cdot$ denotes the product measure. Each point $(x,r)\in\Phi$ corresponds to *(i)* a location $x\in\mathbb{R}^d$ along with *(ii)* a radius $r\in[0,\infty)$ corresponding to the radius of the ball centered around it. We recall that the void probability of the PPP is given by

$$\mathbb{P}(\Phi\cap A=\emptyset)=\exp\big(-\lambda(\ell\times\mu)(A)\big), \tag{1}$$

for any bounded measurable set $A\subset\mathbb{R}^d\times[0,\infty)$.

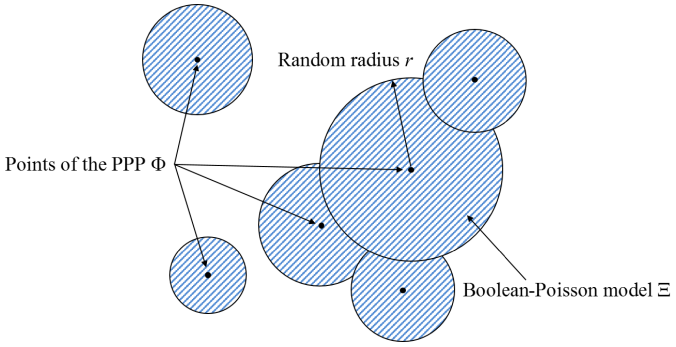

Fig. 1: Illustration of the Boolean-Poisson model.

We denote by $\mathcal{B}_x(r)$ the open Euclidean ball of $\mathbb{R}^d$ centered at $x \in \mathbb{R}^d$ with radius $r \in [0, \infty)$. The occupied space corresponds to the subset of $\mathbb{R}^d$ covered by the balls centered around the points of the PPP, i.e.,

$$\Xi = \bigcup_{(x,r)\in\Phi} \mathcal{B}_x(r), \tag{2}$$

which consists of all points covered by at least one ball. By extension, we will call the set Ξ the Boolean-Poisson model, and Φ is the driving PPP containing the pairs (x, r) of points along with their corresponding radius. In our setting, the Boolean-Poisson model Ξ corresponds to the harvesting energy enabled region (we provide more details in Section III). In other applications, it has been used to model phenomena ranging from the form of geological structures generated by sedimentation to the spread of forest fires. The Boolean-Poisson model has also been used in a wide variety of settings, cf. the summary on pages 67-69 from [7] as well as the applications to wireless communications in [13], [14]. We illustrate the Boolean-Poisson model in Fig. 1.

We now introduce some of the mathematical properties of the model. First, the model is stationary by stationarity of the PPP, and similarly it is also isotropic. In other words, its distribution is invariant with respect to translations and rotations. Second, the metric which will be of interest is the probability that a fixed point in $\mathbb{R}^d$ is covered by the Boolean-Poisson model. The coverage properties have been extensively studied in [9]–[11], and we now briefly recall some basic facts. We consider a point A which is located at $x \in \mathbb{R}^d$ and define the set

$$\mathcal{C}_x = \left\{(y, r) \in \mathbb{R}^d \times [0, \infty) : y \in \mathcal{B}_x(r)\right\}. \tag{3}$$

TABLE I: List of Symbols

Symbol	Definition
Φ	Homogeneous PPP which models the distribution of energy sources
λ	Spatial intensity of energy sources
μ	Distribution of random radius in the Boolean-Poisson model
Ξ	Energy harvesting zone
$\mathcal{P}_H$	Energy harvesting probability
$\mathcal{P}_S$	Transmission success probability
α	Path loss exponent
G	Path loss coefficient
h_k	Fading power of the channel for the k-th hop
g_k	Fading power of the channel between the k-th sensor node and a data sink
P	Transmit power at sensor nodes
γ_k	Received Signal-to-noise ratio (SNR) for the k-th hop
σ^2	Power of additive white Gaussian noise (AWGN)
γ_{th}	SNR threshold

It is readily checked that

$$x \notin \Xi \iff \Phi \cap \mathcal{C}_x = \emptyset, \tag{4}$$

as well as

$$(\ell \times \mu)(\mathcal{C}_x) = \int_0^\infty \Big(\int_{\mathbb{R}^d} \mathbb{1}_{\{y \in \mathcal{B}_x(u)\}} \, \ell(\mathrm{d}y) \Big) \mu(\mathrm{d}u) = \int_0^\infty \ell(\mathcal{B}_x(u)) \mu(\mathrm{d}u). \tag{5}$$

From (1), (4) and (5), the probability that the point A falls in Ξ is easily computed as

$$\begin{aligned} \mathbb{P}(x \in \Xi) &= 1 - \mathbb{P}(\Phi \cap \mathcal{C}_x = \emptyset) = 1 - \exp\left(-\lambda(\ell \times \mu)(\mathcal{C}_x)\right) \\ &= 1 - \exp\left(-\lambda \int_0^\infty \ell(\mathcal{B}_x(u)) \, \mu(\mathrm{d}u)\right) = 1 - \exp\left(-\lambda v_d \int_0^\infty u^d \, \mu(\mathrm{d}u)\right), \end{aligned} \tag{6}$$

where $v_d \triangleq \pi^{d/2} / \Gamma(d/2+1)$ and $\Gamma(\cdot)$ is the Gamma function. We note that $\mathbb{P}(x \in \Xi) = 1$ when $\int_0^\infty u^d \mu(\mathrm{d}u) = \infty$ and as such, we infer that a point in $\mathbb{R}^d$ is almost surely covered by the Boolean-Poisson model if the d-th moment of μ is infinite. Our subsequent analysis will build upon formula (6) expresses the probability that a single node is covered. We will generalize the result in (6) to the case of multiple points $\mathrm{A}_1, \ldots, \mathrm{A}_n$ in Sections IV and V.

III. System Model

In this paper, we analyze the wireless energy harvesting networks consisting of a (random) number of ambient RF energy sources. A list of the symbols used in this paper is given in Table I. The homogeneous PPP Φ with intensity λ models the locations of the ambient RF energy sources. The coverage region of each ambient RF energy source is modeled by an open Euclidean ball of $\mathbb{R}^d$ centered at the location of the energy source. Note that the radius of the coverage region is related to the random signal attenuation over the wireless channel. Therefore, in this paper, we consider a random radius which follows a given distribution μ.

A. General Framework

In this subsection, we develop a general system model which allows for the radii of the Poisson random balls to be distributed according to any distribution $\mu(\mathrm{d}r)$. In Section III-B, we introduce a distribution of radius of the energy harvesting zone which reflects the relation between the harvested power and the path loss of the signals transmitted by the energy sources. By construction, the energy harvesting enabled region is modeled as the Boolean-Poisson model Ξ as defined in (2).

It is worthwhile to note that exploiting the Boolean-Poisson model with random radii to model energy harvesting networks is a new approach and different from the conventional approaches in [21]–[28]. We would like to emphasize that the works in [21]–[28] only concentrated on the probability that a typical node can harvest energy. For networks where multiple nodes communicate with each other, the probability that the nodes can simultaneously harvest power determines the performance of the networks. Therefore, it is important to investigate the performance of the networks where multiple nodes simultaneously scavenge energy.

In this paper, we consider battery-free sensor nodes and a P-threshold based transmission, i.e., a sensor node transmits data with fixed power P when the harvested power at the sensor node exceeds P due to the power regulation [21], [29], [30]. The energy harvesting zone is defined in such a way that a sensor node can harvest power greater than or equal to P when it is located in the energy harvesting zone Ξ.

Let us consider n sensor nodes $\mathrm{A}_1, \mathrm{A}_2, \ldots, \mathrm{A}_n$ which are respectively located at $x_1 \in \mathbb{R}^d, x_2 \in \mathbb{R}^d, \ldots, x_n \in \mathbb{R}^d$. Multi-hop networks are considered, where node A_i transmits data to node A_n aided by nodes $\mathrm{A}_{i+1}, \ldots, \mathrm{A}_{n-1}$. In this paper, for notational brevity, we set $i = 1$. In the networks,

sensor nodes operate in a harvest-then-transmit protocol. More specifically, each sensor node harvests energy one time slot before it transmits or decodes data, and then transmits or decodes data by using the harvested energy. It is additionally assumed that the spatial distribution of energy sources remains the same during the multi-hop transmission, and the energy harvesting and data transmission happen on different spectrum bands. Under this setup, the transmission succeeds when all sensor nodes are located in the energy harvesting enabled region Ξ, and the end-to-end signal-to-noise-ratio (SNR) γ is larger than a certain threshold γ_{th} which is the minimum SNR required for successful data detection.

For $k \in \{2, \ldots, n\}$, we define $\gamma_k \triangleq PGh_k||x_k - x_{k-1}||^{-\alpha}/\sigma^2$ as the received SNR for the $(k-1)$-th hop where P is the transmit power at all sensor nodes, G represents the path loss coefficient, h_k denotes the fading power for the $(k-1)$-th hop, α indicates the path loss exponent, and σ^2 accounts for the power of AWGN. We assume the decode-and-forward (DF) protocol, and therefore the end-to-end SNR $\gamma = \min(\gamma_2, \ldots, \gamma_n)$ is greater than γ_{th} when $\gamma_k \geq \gamma_{th}$ for $k \in \{2, \ldots, n\}$. More formally, let us denote by $\mathcal{P}_H$ and $\mathcal{P}_T$ the probabilities that all nodes can harvest energy and the end-to-end SNR is higher than γ_{th} when all nodes can scavenge energy, respectively. Then, we can express $\mathcal{P}_H$ and $\mathcal{P}_T$ as

$$\mathcal{P}_H \triangleq \mathbb{P}\left(\forall k \in \{1, \ldots, n\},\ x_k \in \Xi\right), \tag{7}$$

and

$$\mathcal{P}_T \triangleq \mathbb{P}\left(\forall k \in \{2, \ldots, n\}, \gamma_k \geq \gamma_{th} \mid \forall k \in \{1, \ldots, n\},\ x_k \in \Xi\right), \tag{8}$$

respectively. The transmission success probability $\mathcal{P}_S$ is then expressed as

$$\mathcal{P}_S \triangleq \mathbb{P}\left(\forall k \in \{1, \ldots, n\},\ x_k \in \Xi,\ \forall i \in \{2, \ldots, n\}, \gamma_i \geq \gamma_{th}\right) = \mathcal{P}_H \mathcal{P}_T. \tag{9}$$

In this paper, the fading powers $\{h_k\}$ are assumed to be independent and identically distributed (i.i.d.) exponential random variables $\mathcal{E}(\tau)$ with parameter τ [31]. It is also assumed that the random variables $\{h_k\}$ are independent of the PPP Φ. Therefore, $\mathcal{P}_T$ can be rewritten as

$$\mathcal{P}_T = \mathbb{P}\left(\forall k \in \{2, \ldots, n\}, \gamma_k \geq \gamma_{th}\right),$$

since the random variables γ_k are independent of Φ (and therefore are also independent of Ξ). We remark that in most of the analysis presented in this paper, the distribution of the fading powers could be generalized to other models (e.g., Nakagami-m or Rician) with only minor

changes in the computation of $\mathcal{P}_S$ in (9); however the results from Section V require the fading powers to be exponentially distributed.

B. Distribution of the radius

In this subsection, we introduce a distribution of the radius which takes the path loss of the signals sent by energy sources into account. First, we investigate the energy harvesting probability in the conventional model in [21]–[25] which considers the aggregated harvested power. Then, we provide a distribution of the radius in the Boolean-Poisson model by investigating the relation between the conventional model and the Boolean-Poisson model.

In the conventional model with the aggregated harvested power, the probability that the harvested power at A_k is larger than the transmit power at sensor nodes P is represented as

$$\Upsilon \triangleq \mathbb{P}\Big(\eta P_e G \sum_{y\in\Phi} h_{y,k}\|x_k - y\|^{-\alpha} \geq P\Big), \tag{10}$$

where η, P_e and $h_{y,k} \sim \mathcal{E}(\tau)$ stand for the RF-to-DC conversion efficiency, the transmit power at energy sources, and the fading power of the channel between A_k and the energy source located at y, respectively. We can obtain a lower bound of the probability in (10) as

$$\Upsilon \geq \mathbb{P}\left(\exists y \in \Phi : \eta P_e G h_{y,k}\|x_k - y\|^{-\alpha} \geq P\right) = \mathbb{P}\left(\exists y \in \Phi : \|x_k - y\| \leq \left(\frac{\eta P_e G h_{y,k}}{P}\right)^{1/\alpha}\right). \tag{11}$$

In the Boolean-Poisson model, the probability that A_k can harvest enough power is written as

$$\mathbb{P}\left(x_k \in \Xi\right) = \mathbb{P}\left(\exists (y,r) \in \Phi : x_k \in \mathcal{B}_y\left(r\right)\right) = \mathbb{P}\left(\exists (y,r) \in \Phi : \|x_k - y\| \leq r\right). \tag{12}$$

By comparing (11) and (12), the energy harvesting probability in the Boolean-Poisson model can be interpreted as a lower bound of the energy harvesting probability in the conventional model when r is distributed as $\left(\frac{\eta P_e G h}{P}\right)^{1/\alpha}$ and $h \sim \mathcal{E}(\tau)$. In other words, if we assume that the radius of the Boolean-Poisson model r is distributed as $\left(\frac{\eta P_e G h}{P}\right)^{1/\alpha}$, the sensor node A_k is covered by the harvesting enabled region Ξ if and only if there exists an energy source located at y such that $\eta P_e G h_{y,k}\|x_k - y\|^{-\alpha} \geq P$, i.e., the energy source positioned at y by itself provides the energy required to power the sensor node.

However, in general, the bound in (11) is not tight, and therefore adopting the above distribution may not be suitable to reflect the aggregated harvested power. In order to take the

aggregated harvested power into account, we introduce a parameter $\delta > 0$ which is designed to satisfy

$$\Upsilon = \mathbb{P}\left(\exists y \in \Phi : \delta\eta P_e G h_{y,k} \|x_k - y\|^{-\alpha} \geq P\right). \tag{13}$$

This is equivalent to assuming that r is distributed according to $\left(\frac{\delta\eta P_e G h}{P}\right)^{1/\alpha}$ for $h \sim \mathcal{E}(\tau)$. It is readily checked that this corresponds to a distribution given by

$$\mu_\delta(\mathrm{d}r) = \frac{\alpha\tau P}{\delta\eta P_e G} r^{\alpha-1} \exp\left(-\frac{\tau P}{\delta\eta P_e G} r^\alpha\right) \mathrm{d}r, \quad r \geq 0. \tag{14}$$

Our initial approach is recovered by setting $\delta = 1$ in the above equation. Under this setup, combining (12) and (13) we observe that the event "A_k is in Ξ" is precisely "there exists an RF source such that δ times the energy harvested from it suffices to power the sensor node".

We now move on to exhibiting δ which satisfies (13). Due to the stationarity of the PPP and [23], we rewrite Υ in (10) as

$$\Upsilon = \int_0^\infty \frac{1}{\pi u} \exp\left(-uP - \frac{2\pi^2\lambda \left(\eta P_e G u/\tau\right)^{\frac{2}{\alpha}}}{\alpha \tan\left(2\pi/\alpha\right)}\right) \sin\left(\frac{2\pi^2\lambda \left(\eta P_e G u/\tau\right)^{\frac{2}{\alpha}}}{\alpha}\right) \mathrm{d}u. \tag{15}$$

Additionally, again by the stationarity of the PPP, we have

$$\begin{aligned}
&\mathbb{P}\left(\exists y \in \Phi : \delta\eta P_e G h_{y,k} \|x_k - y\|^{-\alpha} \geq P\right) = \mathbb{P}\left(\exists y \in \Phi : \delta\eta P_e G h_{y,k} \|y\|^{-\alpha} \geq P\right) \\
&= 1 - \mathbb{P}\left(\forall y \in \Phi : h_{y,k} \leq \frac{P\|y\|^\alpha}{\delta\eta P_e G}\right) = 1 - \mathbb{E}\left[\prod_{y\in\Phi} \mathbb{P}\left(h_{y,k} \leq \frac{P\|y\|^\alpha}{\delta\eta P_e G}\right)\right] \\
&= 1 - \mathbb{E}\left[\prod_{y\in\Phi} \left(1 - \exp\left(-\frac{\tau P\|y\|^\alpha}{\delta\eta P_e G}\right)\right)\right] = 1 - \exp\left(-2\pi\lambda \int_0^\infty \exp\left(-\frac{\tau P r^\alpha}{\delta\eta P_e G}\right) r \,\mathrm{d}r\right) \\
&= 1 - \exp\left(-2\pi\lambda\delta^{2/\alpha} \int_0^\infty \exp\left(-\frac{\tau P \nu^\alpha}{\eta P_e G}\right) \nu \,\mathrm{d}\nu\right).
\end{aligned} \tag{16}$$

By combining (15) and (16), δ which meets the equality in (13), can be identified as

$$\delta = \left(\frac{\ln\left(\frac{1}{1-\Upsilon}\right)}{2\pi\lambda \int_0^\infty \exp\left(-\frac{\tau P \nu^\alpha}{\eta P_e G}\right) \nu \,\mathrm{d}\nu}\right)^{\alpha/2}. \tag{17}$$

Fig. 2 illustrates a realization of the network with $\mu_\delta(\mathrm{d}r)$ in (14) with δ given by (17) where $d = 2$, $\alpha = 3$, $\tau = 1$, $\eta = 1$, $\sigma^2 = -90$ dBm, $P_e = 50$ dBm, $P = -20$ dBm, $G = 0$ dB and $\lambda = 2$ sources/km^2.

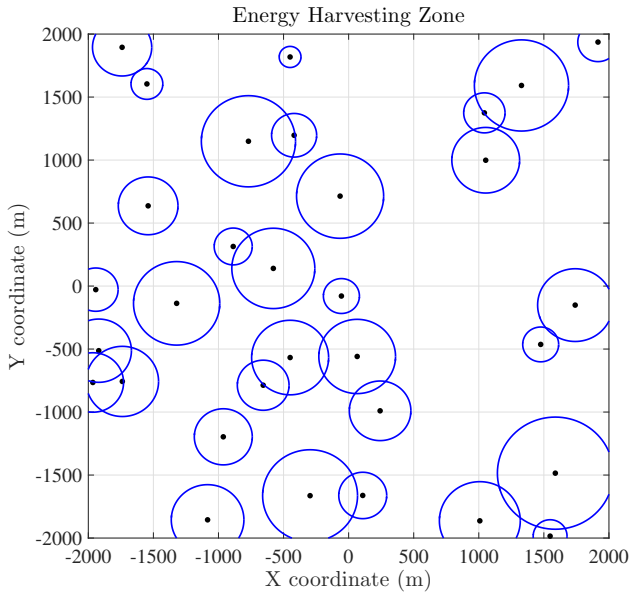

Fig. 2: A realization of the network in a Boolean-Poisson model where dots and circles represent the locations of the ambient RF energy sources and boundaries of the coverage region.

We would like to emphasize that, in the conventional model, it is intractable to analytically investigate the probability that multiple sensor nodes simultaneously scavenge sufficient power. On the contrary, as will be shown in Sections IV and V, in the Boolean-Poisson model, we can derive analytical expressions for the probability that multiple sensor nodes are located in the energy harvesting zone. Lastly, although we have introduced a reasonable choice for the radius distribution in (14), one is free to choose any other distributions according to the problem tackled. Please note that the analytical results in Sections IV and V are valid for any choice of μ.

IV. Performance Analysis for Single-Hop and Multi-Hop Networks

In this section, we first derive an analytical expression for the transmission success probability in single-hop networks with two nodes. Then, we generalize the analytical result to the case of multi-hop networks.

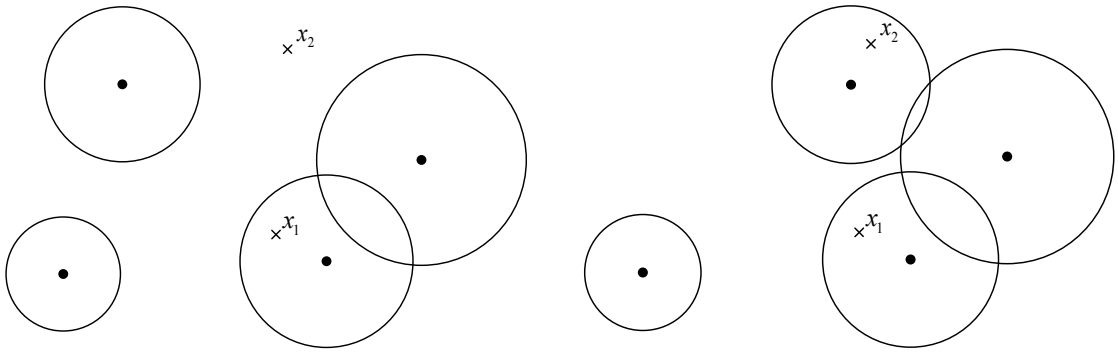

(a) Non-coverage: only A_1 is covered. (b) Coverage: both A_1 and A_2 are covered.

Fig. 3: Examples to illustrate single-hop networks.

A. Single-hop networks

Let us consider two nodes A_1 and A_2 which are located at $x_1 \in \mathbb{R}^d$ and $x_2 \in \mathbb{R}^d$, respectively. Note that both A_1 and A_2 ought to be located in Ξ in order to scavenge energy. As an illustration, the placement of A_2 in Fig. 3a corresponds to a non-coverage situation, whereas that of A_1 and A_2 in Fig. 3b corresponds to a coverage situation.

In networks with two nodes, the coverage probability $\mathcal{P}_H$ in (7) can be rewritten as

$$\mathcal{P}_H = \mathbb{P}\left(x_1 \in \Xi\right) + \mathbb{P}\left(x_2 \in \Xi\right) - \mathbb{P}\left(\{x_1 \in \Xi\} \cup \{x_2 \in \Xi\}\right) \tag{18}$$

$$\overset{\text{(a)}}{=} 2 - 2\exp\left(-\lambda v_d \int_0^\infty u^d \, \mu(\mathrm{d}u)\right) - \mathbb{P}\left(\{x_1 \in \Xi\} \cup \{x_2 \in \Xi\}\right), \tag{19}$$

where (a) follows from (6) and the stationarity of the PPP. In the following theorem, we provide an analytical expression for $\mathcal{P}_H$, in an arbitrary dimension, and for any choice of radius distribution μ.

Theorem 1. *In networks with two nodes, the probability that both nodes can harvest energy is given by*

$$\mathcal{P}_H = 1 - 2\exp\left(-\lambda v_d \int_0^\infty u^d \, \mu(\mathrm{d}u)\right) + \exp\Bigg(- 2\lambda v_d \int_0^\infty u^d \, \mu(\mathrm{d}u) + \lambda v_d \int_{l/2}^\infty I_{1-l^2/(4u^2)}\left(\frac{d+1}{2}, \frac{1}{2}\right) u^d \, \mu(\mathrm{d}u)\Bigg), \tag{20}$$

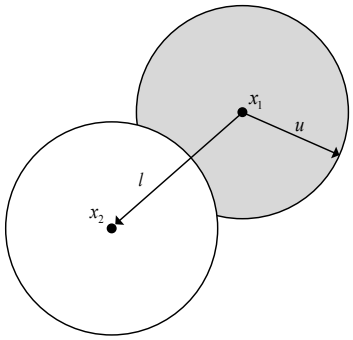

Fig. 4: An illustration for the case of $u \geq l/2$.

where $l \triangleq \|x_1 - x_2\|$ *is the distance between* A_1 *and* A_2*. Here,* $I_z(a,b)$ *is the regularized incomplete beta function defined by*

$$I_z(a,b) = \frac{\Gamma(a+b)\int_0^z u^{a-1}(1-u)^{b-1}\,\mathrm{d}u}{\Gamma(a)\Gamma(b)}, \quad a,b,z>0.$$

Proof. Let us define Φ_{x_1} as a PPP on the same probability space as Φ, supported on the complement $\mathcal{C}_{x_1}^c$ of $\mathcal{C}_{x_1}$, with intensity measure $(\lambda\ell)\times\mu$ restricted to $\mathcal{C}_{x_1}^c$. Recall that $\mathcal{C}_{x_1}$ has been defined in (3). We define accordingly the Boolean-Poisson model associated to Φ_{x_1} as $\Xi_{x_1} = \bigcup_{(x,r)\in\Phi_{x_1}} \mathcal{B}_x(r)$. In a similar manner as in (6) with Φ replaced with Φ_{x_1}, we have

$$\mathbb{P}(x_2 \notin \Xi_{x_1}) = \mathbb{P}\left(\{(y,u)\in\Phi_{x_1} : x_2 \in \mathcal{B}_y(u)\} = \emptyset\right) = \mathbb{P}\left(\Phi_{x_1}\cap\mathcal{C}_{x_2} = \emptyset\right) \tag{21}$$

$$= \exp\left(-\lambda(\ell\times\mu)\left(\mathcal{C}_{x_2}\cap\mathcal{C}_{x_1}^c\right)\right) \tag{22}$$

$$= \exp\Big(-\lambda(\ell\times\mu)\big(\big\{(y,u)\in\mathbb{R}^d\times[0,\infty) : y\in\mathcal{B}_{x_2}(u)\cap\mathcal{B}_{x_1}(u)^c\big\}\big)\Big) \tag{23}$$

$$= \exp\left(-\lambda\int_0^\infty\int_{\mathbb{R}^d}\mathbb{1}_{\left\{y\in\mathcal{B}_{x_2}(u)\cap\mathcal{B}_{x_1}(u)^c\right\}}\,\ell(\mathrm{d}y)\mu(\mathrm{d}u)\right) \tag{24}$$

$$= \exp\left(-\lambda\int_0^\infty \ell\left(\mathcal{B}_{x_2}(u)\cap\mathcal{B}_{x_1}(u)^c\right)\mu(\mathrm{d}u)\right). \tag{25}$$

Now, we focus on the computation of the volume in the above equation. First, if $u < l/2$, then $\ell\left(\mathcal{B}_{x_2}(u)\cap\mathcal{B}_{x_1}(u)^c\right) = \ell\left(\mathcal{B}_{x_2}(u)\right) = v_d u^d$. Second, if $u \geq l/2$, then one has to compute the shaded area in Fig. 4 (represented here in dimension $d=2$). The above d-dimensional volume (known in the literature as hyperspherical cap) is equal to [32]

$$\ell\left(\mathcal{B}_{x_2}(u)\cap\mathcal{B}_{x_1}(u)^c\right) = v_d u^d\left(1 - I_{1-l^2/(4u^2)}\left(\frac{d+1}{2},\frac{1}{2}\right)\right). \tag{26}$$

Hence, combining (25) with (26), we obtain

$$\mathbb{P}\left(x_2 \notin \Xi_{x_1}\right) = \exp\left(-\lambda v_d \int_0^{\infty} u^d \, \mu(\mathrm{d}u) + \lambda v_d \int_{l/2}^{\infty} I_{1-l^2/(4u^2)}\left(\frac{d+1}{2}, \frac{1}{2}\right) u^d \, \mu(\mathrm{d}u)\right). \quad (27)$$

Note that the law of Φ given $\Phi \cap \mathcal{C}_{x_1} = \emptyset$ coincides with the distribution of Φ_{x_1}, and therefore $\mathbb{P}\left(\{x_1 \in \Xi\} \cup \{x_2 \in \Xi\}\right)$ in (19) can be rewritten as

$$\begin{aligned}\mathbb{P}\left(\{x_1 \in \Xi\} \cup \{x_2 \in \Xi\}\right) &= 1 - \mathbb{P}\left(x_1 \notin \Xi\right) \mathbb{P}\left(x_2 \notin \Xi \mid x_1 \notin \Xi\right) \\ &\overset{\text{(b)}}{=} 1 - \mathbb{P}\left(x_1 \notin \Xi\right) \mathbb{P}\left(x_2 \notin \Xi \mid \Phi \cap \mathcal{C}_{x_1} = \emptyset\right) \\ &= 1 - \mathbb{P}\left(x_1 \notin \Xi\right) \mathbb{P}\left(x_2 \notin \Xi_{x_1}\right), \end{aligned} \quad (28)$$

where (b) follows from (4). Combining (19), (27) and (28), we obtain the result in (20). □

In the following corollary, we customize Theorem 1 to the case of $d = 2$ and $\mu_\delta(\mathrm{d}r)$ defined by (14).

Corollary 1. *In the two-dimensional network with two nodes and μ_δ in* (14)*, the coverage probability in* (20) *can be simplified as*

$$\begin{aligned}\mathcal{P}_H = 1 - 2\exp\left(-\lambda\pi\Big(\frac{\delta\eta P_e G}{\tau P}\Big)^{2/\alpha}\Gamma\Big(1+\frac{2}{\alpha}\Big)\right) + \exp\Bigg(-2\lambda\pi\Big(\frac{\delta\eta P_e G}{\tau P}\Big)^{2/\alpha}\Gamma\Big(1+\frac{2}{\alpha}\Big) \\ + \frac{2\lambda\alpha\tau P}{\delta\eta P_e G}\int_{l/2}^{\infty}\left(\arccos\left(\frac{l}{2u}\right) - \frac{l}{2u}\sqrt{1-\frac{l^2}{4u^2}}\right)u^{\alpha+1}\exp\Big(-\frac{\tau P}{\delta\eta P_e G}u^\alpha\Big)\,\mathrm{d}u\Bigg), \end{aligned} \quad (29)$$

where $\arccos(\cdot)$ *denotes the inverse cosine function, and we recall that l is the distance between the nodes* A_1 *and* A_2*. In addition, when $\alpha = 2$, we can obtain a more explicit expression as*

$$\mathcal{P}_H = 1 - 2\exp\left(-\lambda\pi\frac{\delta\eta P_e G}{\tau P}\right) + \exp\left(\frac{\pi\lambda\delta\eta P_e G}{\tau P}\left(\mathrm{erfc}\left(\frac{l}{2}\sqrt{\frac{\tau P}{\delta\eta P_e G}}\right) - 2\right)\right), \quad (30)$$

where $\mathrm{erfc}(x) = \frac{2}{\sqrt{\pi}}\int_x^\infty \mathrm{e}^{-t^2}\,\mathrm{d}t$ *is the complementary error function.*

Proof. By directly exhibiting an anti-derivative, we may rewrite $I_{1-l^2/(4u^2)}\left(\frac{3}{2}, \frac{1}{2}\right)$ as

$$\begin{aligned} I_{1-l^2/(4u^2)}\left(\frac{3}{2}, \frac{1}{2}\right) &= \frac{2}{\pi}\int_0^{1-l^2/(4u^2)} \sqrt{\frac{v}{1-v}}\,\mathrm{d}v = \frac{2}{\pi}\Big[\arccos(\sqrt{1-x}) - \sqrt{1-x}\sqrt{x}\Big]_0^{1-l^2/(4u^2)} \\ &= \frac{2}{\pi}\left(\arccos\left(\frac{l}{2u}\right) - \frac{l}{2u}\sqrt{1-\frac{l^2}{4u^2}}\right). \end{aligned} \quad (31)$$

Also, since $v_2 = \pi$ when $d = 2$, P_H in (20) becomes

$$\mathcal{P}_H = 1 - 2\exp\left(-\lambda\pi\int_0^\infty u^2\,\mu(\mathrm{d}u)\right) + \exp\left(-2\lambda\pi\int_0^\infty u^2\,\mu(\mathrm{d}u) + 2\lambda\int_{l/2}^\infty\left(\arccos\left(\frac{l}{2u}\right) - \frac{l}{2r}\sqrt{1-\frac{l^2}{4u^2}}\right)u^2\,\mu(\mathrm{d}u)\right). \quad (32)$$

Plugging μ_δ in (14) into (32), we compute the integral of u^2 with respect to μ as

$$\int_0^\infty u^2\,\mu_\delta(\mathrm{d}u) = \frac{\alpha\tau P}{\delta\eta P_e G}\int_0^\infty u^{\alpha+1}\exp\Big(-\frac{\tau P}{\delta\eta P_e G}u^\alpha\Big)\,\mathrm{d}u = \Big(\frac{\delta\eta P_e G}{\tau P}\Big)^{2/\alpha}\int_0^\infty y^{2/\alpha}\mathrm{e}^{-y}\,\mathrm{d}y = \Big(\frac{\delta\eta P_e G}{\tau P}\Big)^{2/\alpha}\Gamma\Big(1+\frac{2}{\alpha}\Big), \quad (33)$$

by the change of variables $y = \frac{\tau P}{\delta\eta P_e G}u^\alpha$. We then obtain (29) by combining (32) and (33).

We now focus on the proof of (30). For notational convenience, we define β as $\beta = \tau P/(\delta\eta P_e G)$. By two successive integrations by parts, followed by a change of variable $x = 1/u^2$, we have

$$\begin{aligned}\int_{l/2}^\infty \arccos\Big(\frac{l}{2u}\Big)u^3\exp\big(-\beta u^2\big)\,\mathrm{d}u &= \frac{1}{2\beta}\int_{l/2}^\infty\left(\frac{l}{2\sqrt{1-l^2/(4u^2)}} + 2u\arccos\Big(\frac{l}{2u}\Big)\right)\exp\big(-\beta u^2\big)\,\mathrm{d}u\\ &= \frac{1}{4\beta}\int_{l/2}^\infty\frac{l\exp\big(-\beta u^2\big)}{\sqrt{1-l^2/(4u^2)}}\,\mathrm{d}u + \frac{1}{4\beta^2}\int_{l/2}^\infty\frac{l\exp\big(-\beta u^2\big)}{u^2\sqrt{1-l^2/(4u^2)}}\,\mathrm{d}u\\ &= \frac{1}{4\beta}\int_0^{4/l^2}\frac{x^{-3/2}\exp\big(-\beta/x\big)}{\sqrt{4/l^2-x}}\,\mathrm{d}x + \frac{1}{4\beta^2}\int_0^{4/l^2}\frac{x^{-1/2}\exp\big(-\beta/x\big)}{\sqrt{4/l^2-x}}\,\mathrm{d}x. \quad (34)\end{aligned}$$

Here, by [33, p. 187, eq. (16)], we obtain

$$\frac{1}{4\beta}\int_0^{4/l^2}\frac{x^{-3/2}\exp\big(-\beta/x\big)}{\sqrt{4/l^2-x}}\,\mathrm{d}x = \frac{l\sqrt{\pi}\mathrm{e}^{-\beta l^2/4}}{8\beta^{3/2}}, \quad (35)$$

and by [33, p. 187, eq. (18)], we get

$$\begin{aligned}\frac{1}{4\beta^2}\int_0^{4/l^2}\frac{x^{-1/2}\exp\big(-\beta/x\big)}{\sqrt{4/l^2-x}}\,\mathrm{d}x &= \frac{1}{4\beta^2}\beta^{-1/4}\Big(\frac{4}{l^2}\Big)^{1/4}\mathrm{e}^{-\beta l^2/8}\sqrt{\pi}W_{-1/4,1/4}(\beta l^2/4)\\ &= \frac{\pi}{4\beta^2}\mathrm{erfc}\Big(\frac{\sqrt{\beta}l}{2}\Big), \quad (36)\end{aligned}$$

where W is the Whittaker function. Similarly, by [33, p. 187, eq. (16)] and the change of variables $x = 1/u^2$,

$$\begin{aligned}\int_{l/2}^\infty\frac{l}{2u}\sqrt{1-\frac{l^2}{4u^2}}u^3\exp\Big(-\frac{\tau P}{\delta\eta P_e G}u^2\Big)\,\mathrm{d}u &= \frac{l^2}{8}\int_0^{4/l^2}x^{-5/2}\sqrt{\frac{4}{l^2}-x}\mathrm{e}^{-\beta/x}\,\mathrm{d}x\\ &= \frac{l\sqrt{\pi}\mathrm{e}^{-\beta l^2/4}}{8\beta^{3/2}}. \quad (37)\end{aligned}$$

Combining (34)-(37) with $\beta = \tau P/(\delta\eta P_e G)$, we obtain

$$\int_{l/2}^{\infty}\left(\arccos\left(\frac{l}{2u}\right)-\frac{l}{2u}\sqrt{1-\frac{l^2}{4u^2}}\right)u^3\exp\Big(-\frac{\tau P}{\delta\eta P_e G}u^2\Big)\,\mathrm{d}u = \frac{\pi\delta^2\eta^2P_e^2G^2}{4\tau^2P^2}\mathrm{erfc}\left(\frac{l}{2}\sqrt{\frac{\tau P}{\delta\eta P_e G}}\right).$$

□

From (30), we deduce that the coverage probability is a decreasing function of the distance l. This observation is verified numerically in Fig. 8.

When the networks consist of only two nodes, $\mathcal{P}_T$ in (8) is computed as

$$\mathcal{P}_T = \mathbb{P}\left(\frac{PGh_2 l^{-\alpha}}{\sigma^2} \geq \gamma_{th}\right) = \exp\left(-\frac{\tau l^{\alpha}\sigma^2\gamma_{th}}{PG}\right). \tag{38}$$

From (20), (29) and (38), we can calculate the transmission success probability in (9).

B. Multi-hop networks

In this subsection, we focus on the wireless energy harvesting networks containing multiple aligned nodes. Here, the aligned model for the location of sensor nodes can be applied to various scenarios such as a multi-hop transmission along a straight highway. Let us consider $\mathrm{A}_1, \ldots, \mathrm{A}_n$ nodes ($n \geq 2$) which are located at $x_1 \in \mathbb{R}^d, \ldots, x_n \in \mathbb{R}^d$, respectively, and define the inter-nodal distance as

$$l_{a,b} \triangleq \|x_b - x_a\|, \quad a, b \in \{1, \ldots, n\}. \tag{39}$$

We assume that the nodes are aligned as shown in Fig. 5. In this example, as node A_3 is not covered, node A_3 does not have power available for data decoding and encoding, and therefore outage occurs when node A_1 attempts to communicate with node A_5 through nodes A_2, A_3 and A_4.

We remark that $\mathcal{P}_H$ can be computed as

$$\begin{aligned}\mathbb{P}\left(\forall k \in \{1, \ldots, n\},\ x_k \in \Xi\right) &= 1 - \mathbb{P}\left(\exists k \in \{1, \ldots, n\},\ x_k \notin \Xi\right) \\ &\overset{\text{(c)}}{=} 1 + \sum_{X \subset \{1,\ldots,n\},\ X \neq \emptyset} (-1)^{|X|}\mathbb{P}\left(\forall k \in X,\ x_k \notin \Xi\right), \end{aligned} \tag{40}$$

where (c) follows from the inclusion-exclusion principle and $|X|$ denotes the cardinal of a set X.

We exploit relation (40) in the following theorem, wherein we derive a procedure for computing the probability that all n nodes are covered by the energy harvesting zone.

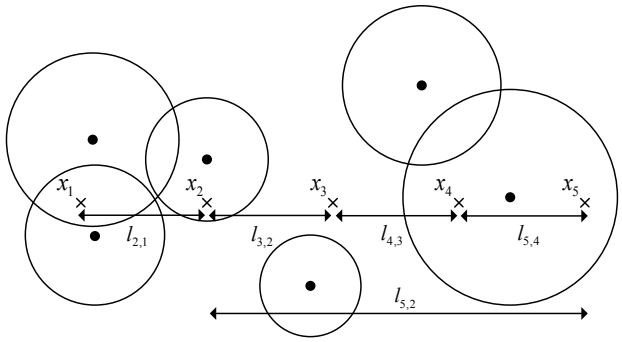

Fig. 5: Illustration of a network with multiple nodes.

Theorem 2. *Let* $X = (a_1, \ldots, a_i) \subset \{1, \ldots, n\}$ *correspond to one of the terms appearing in* (40)*. Then,* $\mathbb{P}\left(\forall k \in X,\ x_k \notin \Xi\right)$ *is given inductively by*

$$\mathbb{P}(\forall k \in \{a_1, \ldots, a_i\},\ x_k \notin \Xi) = \mathbb{P}\left(\forall k \in \{a_1, \ldots, a_{i-1}\},\ x_k \notin \Xi\right) \times \exp\left(- \lambda v_d \int_0^\infty u^d \, \mu(\mathrm{d}u) + \lambda v_d \int_{l_{a_i, a_{i-1}}/2}^\infty I_{1-l_{a_i,a_{i-1}}^2/(4u^2)}\left(\frac{d+1}{2}, \frac{1}{2}\right) u^d \, \mu(\mathrm{d}u)\right), \tag{41}$$

whilst noting that the initial term $\mathbb{P}\left(x_{a_1} \notin \Xi,\ x_{a_2} \notin \Xi\right)$ *has been computed in Theorem 1. Additionally, in the two-dimensional network with* $\mu_\delta(\mathrm{d}r)$ *in* (14)*, the coverage probability is given inductively by*

$$\mathbb{P}(\forall k \in \{a_1, \ldots, a_i\},\ x_k \notin \Xi) = \mathbb{P}\left(\forall k \in \{a_1, \ldots, a_{i-1}\}, x_k \notin \Xi\right) \exp\left(-\lambda\pi\left(\frac{\delta\eta P_e G}{\tau P}\right)^{2/\alpha}\Gamma\left(1+\frac{2}{\alpha}\right) + \frac{2\lambda\alpha\tau P}{\delta\eta P_e G}\int_{l_{a_i,a_{i-1}}/2}^\infty \left(\arccos\left(\frac{l}{2u}\right) - \frac{l}{2u}\sqrt{1-\frac{l^2}{4u^2}}\right) u^{\alpha+1}\exp\left(-\frac{\tau P}{\delta\eta P_e G}u^\alpha\right)\mathrm{d}u\right). \tag{42}$$

Proof. In this setting, in a similar fashion as in (6), one may compute the probability in the

summation in (40) by induction as follows:

$$\begin{aligned}
&\mathbb{P}\left(\forall k \in \{a_1, \ldots, a_i\},\ x_k \notin \Xi\right) \\
&= \mathbb{P}\left(\forall k \in \{a_1, \ldots, a_{i-1}\},\ x_k \notin \Xi\right) \mathbb{P}\left(x_{a_i} \notin \Xi \mid \forall k \in \{a_1, \ldots, a_{i-1}\},\ x_k \notin \Xi\right) && (43) \\
&\overset{\text{(d)}}{=} \mathbb{P}\left(\forall k \in \{a_1, \ldots, a_{i-1}\},\ x_k \notin \Xi\right) \mathbb{P}\left(x_{a_i} \notin \Xi \mid \Phi \cap \mathcal{C}_{x_{a_1}} = \emptyset, \ldots, \Phi \cap \mathcal{C}_{x_{a_{i-1}}} = \emptyset\right) && (44) \\
&= \mathbb{P}\left(\forall k \in \{a_1, \ldots, a_{i-1}\},\ x_k \notin \Xi\right) \exp\left(-\lambda(\ell \times \mu)\left(\mathcal{C}_{x_{a_i}} \cap (\mathcal{C}_{x_{a_1}} \cup \cdots \cup \mathcal{C}_{x_{a_{i-1}}})^c\right)\right) && (45) \\
&= \mathbb{P}\left(\forall k \in \{a_1, \ldots, a_{i-1}\},\ x_k \notin \Xi\right) \\
&\qquad \times \exp\left(-\lambda \int_0^\infty \ell\big(\mathcal{B}_{x_{a_i}}(u) \cap \mathcal{B}_{x_{a_1}}(u)^c \cap \cdots \cap \mathcal{B}_{x_{a_{i-1}}}(u)^c\big)\mu(\mathrm{d}u)\right), && (46)
\end{aligned}$$

where we obtain (d) by applying (4). From the assumption that the n nodes are aligned, we have

$$\mathcal{B}_{x_{a_i}}(u) \cap \mathcal{B}_{x_{a_1}}(u)^c \cap \cdots \cap \mathcal{B}_{x_{a_{i-1}}}(u)^c = \mathcal{B}_{x_{a_i}}(u) \cap \mathcal{B}_{x_{a_{i-1}}}(u)^c. \tag{47}$$

Thus, by proceeding as in Theorem 1, when $u < l_{a_i,a_{i-1}}/2$, we obtain

$$\ell\left(\mathcal{B}_{x_{a_i}}(u) \cap \mathcal{B}_{x_{a_{i-1}}}(u)^c\right) = \ell\left(\mathcal{B}_{x_{a_i}}(u)\right) = v_d u^d, \tag{48}$$

while, when $u \geq l_{a_i,a_{i-1}}/2$, the volume can be computed as

$$\ell\left(\mathcal{B}_{x_{a_i}}(u) \cap \mathcal{B}_{x_{a_{i-1}}}(u)^c\right) = v_d u^d\left(1 - I_{1-l_{a_i,a_{i-1}}^2/(4u^2)}\left(\frac{d+1}{2}, \frac{1}{2}\right)\right). \tag{49}$$

The result in (42) follows by applying the same arguments as in the proof of Corollary 1. □

In multi-hop networks, $\mathcal{P}_T$ in (8) becomes

$$\mathcal{P}_T = \mathbb{P}\left(\forall k \in \{2, \ldots, n\}, \frac{PGh_k l_{k,k-1}^{-\alpha}}{\sigma^2} \geq \gamma_{th}\right) = \exp\left(-\frac{\tau\sigma^2\gamma_{th}}{PG}\sum_{k=2}^{n} l_{k,k-1}^{\alpha}\right). \tag{50}$$

We may then derive the transmission success probability $\mathcal{P}_S$ in (9) using Theorem 2, along with (40) and (50).

C. Multi-hop networks with sensor nodes distributed according to a point process

In the above subsections, the aligned sensor nodes have fixed distances. In this subsection, we consider aligned sensor nodes distributed according to a point process Ψ taking values in $[0, L]$, where $L > 0$ is fixed, and independent from Φ. Recall that Φ is the underlying PPP representing the ambient RF energy sources. More specifically, the location of the node A_0 is fixed as 0, and another node A_N is assumed to be located at a distance L from A_0. Between A_0 and A_N, other

nodes are assumed to be distributed according to Ψ. We assume that Ψ has a density f_Ψ with respect to the Poisson point process on $[0, L]$ with intensity 1, i.e., by definition,

$$\mathbb{E}\big[g(\Psi)\big] = \sum_{n\geq 0} \frac{\mathrm{e}^{-L}}{n!} \int_0^L \cdots \int_0^L g(\{t_1, \ldots, t_n\}) f_\Psi(\{t_1, \ldots, t_n\})\, \mathrm{d}t_1 \cdots \mathrm{d}t_n, \tag{51}$$

for all non-negative functions g depending on a subset of points of $[0, L]$. In the above definition, the points $t_1, \ldots, t_n$ represent the positions of the sensor nodes, which are located between 0 and L. When Ψ is a PPP on $[0, L]$ with intensity λ_s, we have

$$f_\Psi(\{t_1, \ldots, t_n\}) = \lambda_s^n \exp(L(1 - \lambda_s)), \tag{52}$$

but most other choices of point processes fit into this subsection's framework.

When $\Psi = \{t_1, \ldots, t_n\}$, the SNR for the last hop can be written by

$$\gamma_N \triangleq \begin{cases} PGh_N L^{-\alpha}/\sigma^2 & \text{if } \Psi = \emptyset, \\ PGh_N (L - t_{(n)})^{-\alpha}/\sigma^2 & \text{otherwise,} \end{cases} \tag{53}$$

and the SNR for the k-th hop becomes

$$\gamma_k \triangleq \begin{cases} PGh_1 t_{(1)}^{-\alpha}/\sigma^2 & \text{if } k = 1, \\ PGh_k (t_{(k)} - t_{(k-1)})^{-\alpha}/\sigma^2 & \text{otherwise,} \end{cases} \tag{54}$$

where $(t_{(1)}, \ldots, t_{(n)})$ is the ordered version of the points of Ψ, i.e., the n-tuple such that $t_{(1)} < \cdots < t_{(n)}$. The transmission success probability in this model is given by

$$\mathcal{P}_S = \mathbb{P}(\mathrm{A}_0 \in \Xi,\ \mathrm{A}_N \in \Xi,\ \gamma_N \geq \gamma_{th},\ \forall t_i \in \Psi,\ \mathrm{A}_i \in \Xi \text{ and } \gamma_i \geq \gamma_{th}). \tag{55}$$

From (51) and the independence of Ψ and Φ, the above probability is computed as

$$\begin{aligned} \mathcal{P}_S =& \mathbb{P}(\mathrm{A}_0 \in \Xi,\ \mathrm{A}_N \in \Xi,\ \gamma_N \geq \gamma_{th},\ \Psi = \emptyset) + \sum_{n\geq 1} \frac{\mathrm{e}^{-L}}{n!} \int_0^L \cdots \int_0^L f_\Psi(\{t_1, \ldots, t_n\}) \qquad (56) \\ & \times \mathbb{P}(\mathrm{A}_0 \in \Xi,\ \mathrm{A}_N \in \Xi,\ \gamma_N \geq \gamma_{th},\ \forall i = 1, \ldots, n,\ t_i \in \Xi \text{ and } \gamma_i \geq \gamma_{th})\, \mathrm{d}t_1 \cdots \mathrm{d}t_n \\ =& \sum_{n\geq 1} \frac{\mathrm{e}^{-L}}{n!} \int_0^L \cdots \int_0^L \mathbb{P}(\mathrm{A}_0 \in \Xi,\ \mathrm{A}_N \in \Xi,\ \forall i = 1, \ldots, n,\ t_i \in \Xi) \mathbb{P}(\gamma_N \geq \gamma_{th}) \qquad (57) \\ & \times \prod_{i=1}^n \mathbb{P}(\gamma_i \geq \gamma_{th}) f_\Psi(\{t_1, \ldots, t_n\})\, \mathrm{d}t_1 \cdots \mathrm{d}t_n + \mathbb{P}(\mathrm{A}_0 \in \Xi,\ \mathrm{A}_N \in \Xi,\ \gamma_N \geq \gamma_{th},\ \Psi = \emptyset) \\ =& \mathbb{P}(\mathrm{A}_0 \in \Xi,\ \mathrm{A}_N \in \Xi,\ \gamma_N \geq \gamma_{th},\ \Psi = \emptyset) \qquad (58) \end{aligned}$$

$$+\sum_{n\geq 1}\frac{\mathrm{e}^{-L}}{n!}\int_0^L\cdots\int_0^L \mathbb{P}(\mathrm{A}_0\in\Xi,\ \mathrm{A}_N\in\Xi,\ \forall i=1,\ldots,n,\ t_i\in\Xi)f_\Psi(\{t_1,\ldots,t_n\})$$
$$\times\exp\bigg(-\frac{\tau\gamma_{th}\sigma^2}{PG}\Big((L-t_{(n)})^\alpha+t_{(1)}^\alpha+\sum_{i=2}^n(t_{(i)}-t_{(i-1)})^\alpha\Big)\bigg)\,\mathrm{d}t_1\cdots\mathrm{d}t_n.$$

Additionally, the first term on the right-hand side of equation (58) has already been computed in Section IV-A; specifically,

$$\begin{aligned}
&\mathbb{P}(\mathrm{A}_0\in\Xi,\ \mathrm{A}_N\in\Xi,\ \gamma_N\geq\gamma_{th},\ \Psi=\emptyset)\\
&=\mathbb{P}(\mathrm{A}_0\in\Xi,\ \mathrm{A}_N\in\Xi,\ \gamma_N\geq\gamma_{th}\mid\Psi=\emptyset)\mathbb{P}(\Psi=\emptyset) &(59)\\
&=\ f_\Psi(\emptyset)\exp\Big(-\frac{\tau\gamma_{th}\sigma^2L^\alpha}{PG}-L\Big)\bigg(1-2\exp\Big(-\lambda v_d\int_0^\infty u^d\,\mu(\mathrm{d}u)\Big) &(60)\\
&\qquad+\exp\bigg(-2\lambda v_d\int_0^\infty u^d\,\mu(\mathrm{d}u)+\lambda v_d\int_{L/2}^\infty I_{1-\frac{L^2}{4u^2}}\Big(\frac{d+1}{2},\frac{1}{2}\Big)\,u^d\,\mu(\mathrm{d}u)\bigg)\bigg),
\end{aligned}$$

by Theorem 1. Here, we can calculate $\mathbb{P}(\Psi=\emptyset)$ by applying (51) with $g(\Psi)=\mathbb{1}_{\{\Psi=\emptyset\}}$. In addition, the integrand in (58) is computed recursively by Theorem 2.

Lastly, the second term in (58) can be rewritten as a series of integral on $[0,1]^n$ by the change of variables $s_i\equiv t_i/L$ for $i=1,\ldots,n$; namely it is equal to

$$\sum_{n\geq 1}\frac{L^n\mathrm{e}^{-L}}{n!}\int_0^1\cdots\int_0^1 \mathbb{P}(\mathrm{A}_0\in\Xi,\ \mathrm{A}_N\in\Xi,\ \forall i=1,\ldots,n,\ Ls_i\in\Xi)f_\Psi(\{Ls_1,\ldots,Ls_n\})$$
$$\times\exp\bigg(-\frac{\tau\gamma_{th}\sigma^2L^\alpha}{PG}\Big((1-s_{(n)})^\alpha+s_{(1)}^\alpha+\sum_{i=2}^n(s_{(i)}-s_{(i-1)})^\alpha\Big)\bigg)\,\mathrm{d}s_1\cdots\mathrm{d}s_n. \quad (61)$$

Then, by considering only the first N_{max} terms, an approximation of (61) can be written as

$$\sum_{n=1}^{N_{max}}\frac{L^n\mathrm{e}^{-L}}{n!}\int_0^1\cdots\int_0^1 \mathbb{P}(\mathrm{A}_0\in\Xi,\ \mathrm{A}_N\in\Xi,\ \forall i=1,\ldots,n,\ Ls_i\in\Xi)f_\Psi(\{Ls_1,\ldots,Ls_n\})$$
$$\times\exp\bigg(-\frac{\tau\gamma_{th}\sigma^2L^\alpha}{PG}\Big((1-s_{(n)})^\alpha+s_{(1)}^\alpha+\sum_{i=2}^n(s_{(i)}-s_{(i-1)})^\alpha\Big)\bigg)\,\mathrm{d}s_1\cdots\mathrm{d}s_n, \quad (62)$$

which is the approximation that we exploit in our numerical analysis, see Fig. 13.

Since the n-fold integrals appearing in the summation (62) lead to an extremely high computational complexity, we utilize the QMC integration method for efficient numerical integration. We refer the reader to Section VI-A for details on the QMC method.

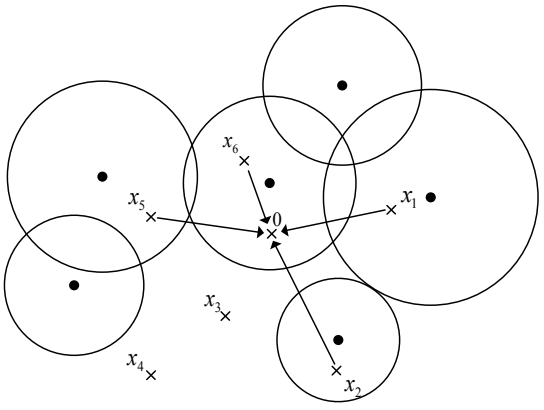

Fig. 6: An example to illustrate networks with star-shaped topology.

V. STAR-SHAPED TOPOLOGY

We now study a network consisting of a data collector and n sensor nodes. Let us consider a data collector A_0 located at 0 and n sensor nodes $\mathrm{A}_1, \mathrm{A}_2, \ldots, \mathrm{A}_n$, which are respectively located at $x_1 \in \mathbb{R}^d, x_2 \in \mathbb{R}^d, \ldots, x_n \in \mathbb{R}^d$ and transmit data to the data collector. We assume that the data collector adopts a successive interference cancellation technique for information decoding as in [34]. Then, the throughput is written as

$$C \triangleq \log_2 \left(1 + \sum_{k=1}^{n} \frac{PGg_k}{\sigma^2 \|x_k\|^\alpha} \mathbb{1}_{\{\mathrm{A}_0 \in \Xi,\ \mathrm{A}_k \in \Xi\}} \right), \tag{63}$$

where $g_k \sim \mathcal{E}(\tau)$ is the fading power of the channel between the data collector and the k-th sensor node, and $\{g_k\}$ are independent. In the following, we denote by $\Theta_{\text{all}} = \{1, \ldots, n\}$ the set of indices of sensor nodes. Since g_k is independent of Ξ, we have

$$\mathbb{E}[C] = \sum_{\Theta \subset \Theta_{\text{all}}} \mathbb{E}\left[C \mathbb{1}_{\{\mathrm{A}_0 \in \Xi,\ \forall k \in \Theta, \mathrm{A}_k \in \Xi,\ \forall i \in \Theta_{\text{all}} \setminus \Theta, \mathrm{A}_i \notin \Xi\}} \right] \tag{64}$$

$$= \sum_{\Theta \subset \Theta_{\text{all}}} \mathbb{E}\left[\log_2 \left(1 + \sum_{k \in \Theta} \frac{PGg_k}{\sigma^2 \|x_k\|^\alpha} \right) \mathbb{1}_{\{\mathrm{A}_0 \in \Xi,\ \forall k \in \Theta, \mathrm{A}_k \in \Xi,\ \forall i \in \Theta_{\text{all}} \setminus \Theta, \mathrm{A}_i \notin \Xi\}} \right] \tag{65}$$

$$= \sum_{\Theta \subset \Theta_{\text{all}}} \mathbb{E}\left[\log_2 \left(1 + \sum_{k \in \Theta} \frac{PGg_k}{\sigma^2 \|x_k\|^\alpha} \right) \right] \times \mathbb{P}\left(\mathrm{A}_0 \in \Xi,\ \forall k \in \Theta,\ \mathrm{A}_k \in \Xi,\ \forall i \in \Theta_{\text{all}} \setminus \Theta,\ A_i \notin \Xi \right). \tag{66}$$

In (66), Θ is assumed to be non-empty since otherwise $\log_2 \left(1 + \sum_{k \in \Theta} \frac{PGg_k}{\sigma^2 \|x_k\|^\alpha} \right) = 0$, i.e., the corresponding term does not appear. Let $\Theta = \{\theta_1, \ldots, \theta_m\} \subset \Theta_{\text{all}}$, for some $m \geq 1$. In general,

it is intractable to identify a closed-form expression for $\mathbb{P}(\mathrm{A}_0 \in \Xi,\ \forall k \in \Theta,\ \mathrm{A}_k \in \Xi,\ \forall i \in \Theta_{\text{all}} \setminus \Theta,\ A_i \notin \Xi)$. However, when the events $\{\mathrm{A}_0 \in \Xi,\ \mathrm{A}_{\theta_1} \in \Xi\}$ and $\{\mathrm{A}_{\theta_k} \in \Xi\}$ are close to being mutually independent as k spans $\{2, \ldots, m\}$, the following approximation holds:

$$\mathbb{P}\left(\mathrm{A}_0 \in \Xi,\ \forall k \in \Theta,\ \mathrm{A}_k \in \Xi,\ \forall i \in \Theta_{\text{all}} \setminus \Theta,\ A_i \notin \Xi\right) \approx \mathbb{P}\left(\mathrm{A}_0 \in \Xi,\ \mathrm{A}_{\theta_1} \in \Xi\right) \times \prod_{k=2}^{m} \mathbb{P}\left(\mathrm{A}_{\theta_k} \in \Xi\right) \prod_{i \in \Theta_{\text{all}} \setminus \Theta} \left(1 - \mathbb{P}\left(\mathrm{A}_i \in \Xi\right)\right). \quad (67)$$

Here, $\mathbb{P}\left(\mathrm{A}_{\theta_k} \in \Xi\right)$ and $\mathbb{P}\left(\mathrm{A}_0 \in \Xi,\ \mathrm{A}_{\theta_1} \in \Xi\right)$ in (67) can be computed by the results in (6) and (20), respectively. Although the equation (67) is an approximation, from Figs. 14 and 15 in Section VI, we have confirmed that the approximation is tight.

We now concentrate on the factor $\mathbb{E}\left[\log_2\left(1 + \sum_{k\in\Theta} \frac{PGg_k}{\sigma^2\|x_k\|^\alpha}\right)\right]$ in (66). Let us define X_k as a series of independent exponential random variables with parameters $\tau\sigma^2\|x_k\|^\alpha/(PG)$. Then, we have

$$\sum_{k\in\Theta} \frac{PGg_k}{\sigma^2\|x_k\|^\alpha} = \sum_{k\in\Theta} X_k.$$

By [35, Lemma 1], we obtain

$$\mathbb{E}\left[\log_2\left(1 + \sum_{k\in\Theta} \frac{PGg_k}{\sigma^2\|x_k\|^\alpha}\right)\right] = \int_0^\infty \frac{1 - \prod_{k\in\Theta}(1 + zPG(\tau\sigma^2\|x_k\|^\alpha)^{-1})^{-1}}{z\ln(2)} \mathrm{e}^{-z}\ \mathrm{d}z, \quad (68)$$

which provides an approximation of $\mathbb{E}[C]$ when combined with (66) and (67).

Next, we introduce an explicit expression of $\mathbb{E}\left[\log_2\left(1 + \sum_{k\in\Theta} \frac{PGg_k}{\sigma^2\|x_k\|^\alpha}\right)\right]$, which does not require the numerical integration in (68), for the case with $\|x_1\| = \cdots = \|x_k\| \triangleq \|x\|$ for some fixed x. Assume first that $\Theta = \{\theta\}$ is a singleton for a fixed $\theta \in \Theta_{\text{all}}$. Then,

$$\mathbb{E}\left[\log_2\left(1 + \sum_{k\in\Theta} \frac{PGg_k}{\sigma^2\|x_k\|^\alpha}\right)\right] = \int_0^\infty \log_2\left(1 + \frac{PGu}{\sigma^2\|x_\theta\|^\alpha}\right) \tau\mathrm{e}^{-\tau u}\ \mathrm{d}u \quad (69)$$

$$= \left[-\log_2\left(1 + \frac{PGu}{\sigma^2\|x_\theta\|^\alpha}\right)\mathrm{e}^{-\tau u}\right]_0^\infty + \int_0^\infty \frac{\mathrm{d}}{\mathrm{d}u}\left(\log_2\left(1 + \frac{PGu}{\sigma^2\|x_\theta\|^\alpha}\right)\right)\mathrm{e}^{-\tau u}\ \mathrm{d}u \quad (70)$$

$$= \frac{PG}{\ln(2)\sigma^2\|x_\theta\|^\alpha} \int_0^\infty \frac{1}{1 + \frac{PGu}{\sigma^2\|x_\theta\|^\alpha}} \mathrm{e}^{-\tau u}\ \mathrm{d}u \quad (71)$$

$$\overset{\text{(e)}}{=} \frac{\mathrm{e}^{\tau\sigma^2\|x_\theta\|^\alpha/(PG)}}{\ln(2)} \int_1^\infty \frac{1}{v} \mathrm{e}^{-v\tau\sigma^2\|x_\theta\|^\alpha/(PG)}\ \mathrm{d}v \quad (72)$$

$$= \frac{\mathrm{e}^{\tau\sigma^2\|x_\theta\|^\alpha/(PG)}}{\ln(2)} \mathrm{E}_1\left(\frac{\tau\sigma^2\|x_\theta\|^\alpha}{PG}\right), \quad (73)$$

where we have used the change of variable $v = 1 + uPG\sigma^{-2}\|x_\theta\|^{-\alpha}$ in (e), and

$$\mathrm{E}_n(x) \triangleq \int_1^\infty \frac{1}{u^n}\mathrm{e}^{-xu}\,\mathrm{d}u, \quad x \neq 0,\ n \geq 1, \tag{74}$$

is a generalization of the exponential integral special function. For a non-singleton $\Theta = \{\theta_1, \ldots, \theta_m\} \subset \Theta_{\text{all}}$, we note that $\sum_{k\in\Theta} g_k$ is distributed according to a gamma random variable with shape parameter m and rate parameter τ. In this case,

$$\mathbb{E}\left[\log_2\left(1+\sum_{k\in\Theta}\frac{PGg_k}{\sigma^2\|x_k\|^\alpha}\right)\right] = \underbrace{\frac{\tau^m}{(m-1)!}\int_0^\infty \log_2\left(1+\frac{PGr}{\sigma^2\|x\|^\alpha}\right) r^{m-1}\mathrm{e}^{-\tau r}\,\mathrm{d}r}_{:=I_m}, \tag{75}$$

and I_m satisfies the following recursion:

$$\begin{aligned}
I_m &= \frac{\tau^{m-1}}{(m-1)!\ln(2)}\int_0^\infty\left(\ln\left(1+\frac{PGr}{\sigma^2\|x\|^\alpha}\right)(m-1)r^{m-2} + \frac{PG}{\sigma^2\|x\|^\alpha\left(1+\frac{PGr}{\sigma^2\|x\|^\alpha}\right)}r^{m-1}\right)\mathrm{e}^{-\tau r}\mathrm{d}r \\
&= I_{m-1} + \frac{\tau^{m-1}}{(m-1)!\ln(2)}\int_0^\infty \frac{1}{\sigma^2\|x\|^\alpha/(PG)+r}r^{m-1}\mathrm{e}^{-\tau r}\,\mathrm{d}r \\
&= I_{m-1} + \frac{1}{(m-1)!\ln(2)}\int_0^\infty \frac{1}{\tau\sigma^2\|x\|^\alpha/(PG)+u}u^{m-1}\mathrm{e}^{-u}\,\mathrm{d}u \\
&\overset{\text{(f)}}{=} I_{m-1} + \frac{\mathrm{e}^{\tau\sigma^2\|x\|^\alpha/(PG)}}{\ln(2)}\mathrm{E}_m\left(\frac{\tau\sigma^2\|x\|^\alpha}{PG}\right),
\end{aligned}$$

where (f) follows from Lemma 1 in the appendix. Consequently, from (73) and (75), we have

$$\mathbb{E}\left[\log_2\left(1+\sum_{k\in\Theta}\frac{PGg_k}{\sigma^2\|x_k\|^\alpha}\right)\right] = \frac{\mathrm{e}^{\tau\sigma^2\|x\|^\alpha/(PG)}}{\ln(2)}\sum_{k=1}^{m}\mathrm{E}_k\left(\frac{\tau\sigma^2\|x\|^\alpha}{PG}\right), \tag{76}$$

where we recall that m is the number of elements in Θ, and E_k has been defined in (74).

Combining (66) and (76) with the approximation (67), we approximate the average throughput as

$$\begin{aligned}
\mathbb{E}[C] \approx \frac{\mathrm{e}^{\tau\sigma^2\|x\|^\alpha/(PG)}}{\ln(2)} \sum_{\Theta\subset\Theta_{\text{all}};\ \Theta\neq\emptyset}\ \sum_{k=1}^{|\Theta|}\mathrm{E}_k\left(\frac{\tau\sigma^2\|x\|^\alpha}{PG}\right)\mathbb{P}\left(\mathrm{A}_0\in\Xi,\ \mathrm{A}_{\theta_m}\in\Xi\right) \\
\times \prod_{k\in\Theta;\ k\neq\theta_m}\mathbb{P}\left(\mathrm{A}_k\in\Xi\right)\prod_{i\in\Theta_{\text{all}}\setminus\Theta}\left(1-\mathbb{P}\left(\mathrm{A}_i\in\Xi\right)\right),
\end{aligned} \tag{77}$$

where $|\Theta|$ denotes the cardinality of Θ and $\theta_m \triangleq \min\Theta$ for any non-empty $\Theta \subset \Theta_{\text{all}}$.

VI. Simulation Results

In this section, we put forth numerical simulations to validate our analytical results.

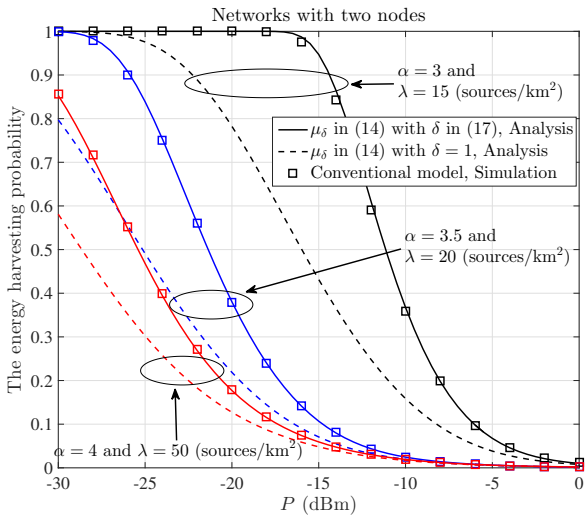

Fig. 7: Comparison between the Boolean-Poisson model and the conventional model.

A. *Simulation framework*

Unless otherwise stated, we assume that $d = 2$, $\alpha = 3$, $\tau = 1$, $\eta = 1$, $\sigma^2 = -90$ dBm, $G = 0$ dB, and $P_e = 50$ dBm, and adopt the distribution of radius μ_δ in (14) with δ given by (17). We use the lines and symbols to denote the analytical and simulated results, respectively. Simulation results are averaged over 10^5 realizations of the channel, the locations of the nodes and the radii of coverage regions.

We now recall some background about QMC integration (see also [36] for a gentle introduction). The QMC integration method consists in finding a deterministic sequence $\mathbf{x}_1, \ldots \mathbf{x}_{N_{\text{sample}}} \in [0,1]^n$ such that

$$Q_{N_{\text{sample}}}(f) := \sum_{m=1}^{N_{\text{sample}}} w_m f(\mathbf{x}_m) \approx \int_{[0,1]^n} f(\mathbf{x})\, \mathrm{d}\mathbf{x}, \quad \text{for all } f : [0,1]^n \to \mathbb{C} \text{ continuous}, \tag{78}$$

as N_{sample} goes to infinity. In our simulations, we employ the Sobol sequence [37]. As expected, the tightness of the QMC method depends on the number of samples N_{sample}. We have confirmed from computer simulations that the QMC method with more than 32 samples yields only negligible performance gain when evaluating our analytical result in (61). Therefore, in this paper, we set the number of samples for the QMC method to $N_{\text{sample}} = 32$.

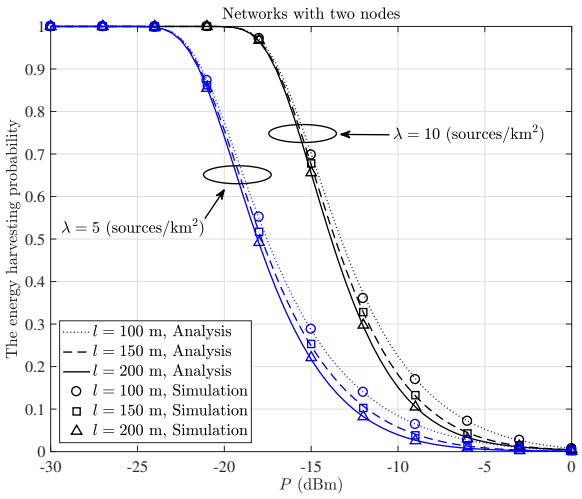

Fig. 8: Comparison of the energy harvesting probability for the single-hop networks.

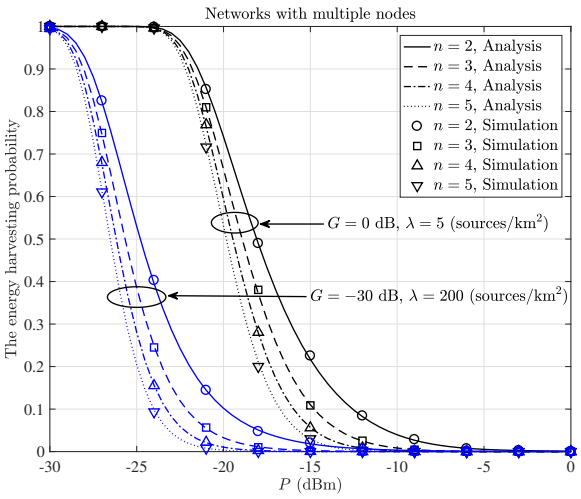

Fig. 9: Comparison of the energy harvesting probability for the multi-hop networks.

B. Single-hop and multi-hop networks

Figs. 7 to 9 illustrate the energy harvesting probability $\mathcal{P}_H$ of the networks. In Fig. 7, we evaluate $\mathcal{P}_H$ for the single-hop networks where $l = 150$ m, and in Fig. 9, $l_{a,a+1}$ = 200 m for $a = 1, \ldots, n-1$. In Fig. 7, the conventional model means the model which is based on the aggregated harvested power [21]–[25]. As shown in Fig. 7, when the distribution (14) with δ given by (17) is employed, our analysis for the Boolean-Poisson model in Theorem 1 exhibits almost identical performance with the conventional model for different values of α and λ. Hence, in Figs 8 to 15, we adopt the distribution in (14) with δ given by (17). From Figs. 8 and 9, it is shown that the analytical results in Section IV match well with the simulated results and the energy harvesting probability decreases as P increases. When the sensor nodes in the network are close together, the sensor nodes are more likely to be located in a coverage region of an RF source, and therefore the probability that the nodes are in the energy harvesting zone becomes high. Therefore, in Fig. 8, we observe that the energy harvesting probability increases as the distance between two nodes l becomes small. Also, in Fig. 9, it is shown that the energy harvesting probability decays as the number of sensor nodes increases.

In Figs. 10 and 11, we evaluate the transmission success probability $\mathcal{P}_S$ of the networks. In Fig. 10, the distance between nodes l is set to $l = 200$ m, and in Fig. 11, the intensity λ is fixed

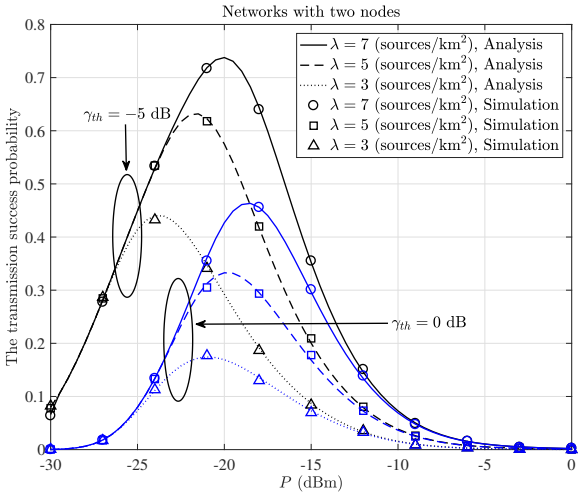

Fig. 10: Comparison of the transmission success probability for the single-hop networks.

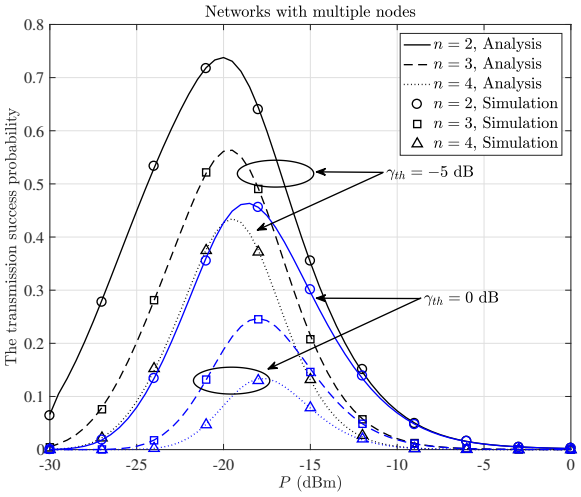

Fig. 11: Comparison of the transmission success probability for the multi-hop networks.

as $\lambda = 7$ sources/km^2 and $l_{a,a+1}$ = 200 m for $a = 1, \ldots, n-1$. As expected, $\mathcal{P}_S$ increases as γ_{th} decreases. One interesting observation is that $\mathcal{P}_S$ is not a monotonic function of P. This is due to the fact that the energy harvesting probability $\mathcal{P}_H$ is a decreasing function of P while $\mathcal{P}_T$ in (50) is an increasing function of P. From the observation that $\mathcal{P}_S$ becomes larger as P grows when P is small, we can refer that $\mathcal{P}_s$ is dominated by $\mathcal{P}_T$ when P is low. Moreover, in Fig. 10, it is shown that $\mathcal{P}_S$ grows as the intensity λ becomes larger.

Fig. 12 demonstrates the optimal number of hops for the networks with multiple nodes where $\gamma_{th} = -5$ dB. We assume that there are $n > 1$ aligned nodes spanning a given distance $L > 0$. We further assume that the inter-nodal distance is fixed and equal to $L/(n-1)$, i.e., $l_{i,i+1} = L/(n-1)$ for all $i \in \{1, \ldots, n-1\}$. Then, the optimal number of hops, which maximizes $\mathcal{P}_S = \mathcal{P}_T \mathcal{P}_H$, is identified by employing the exhaustive search algorithm. Note that when the number of hops increases, $\mathcal{P}_H$ decreases whereas $\mathcal{P}_T$ increases since the received SNR at each hop largely increases due to the shortened distance. Therefore, there exists a trade-off between $\mathcal{P}_H$ and $\mathcal{P}_T$, from which an optimal number of hops can be obtained. Note that $\mathcal{P}_H$ gets higher as P decreases or λ increases. Therefore, as shown in Fig. 12, when P decays or λ grows, the optimal number of hops is increased since $\mathcal{P}_H$ slowly decreases over the number of hops. Also, when L is large, due to a large path loss between the source (A_1) and the destination (A_n), $\mathcal{P}_T$ is very low for a small number of hops. Thus, in order to improve $\mathcal{P}_T$, the optimal number of hops becomes

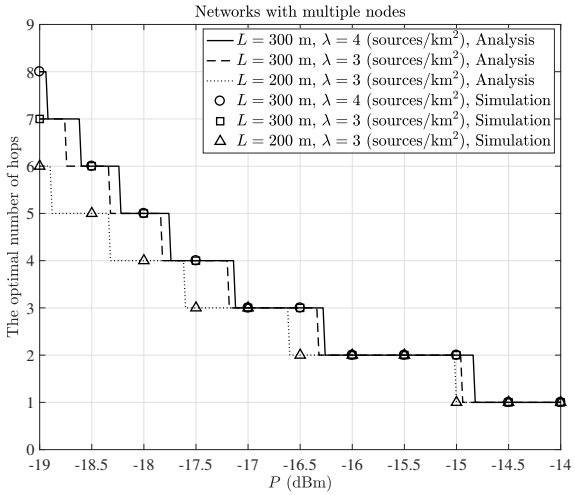

Fig. 12: Comparison of the optimal number of hops for the multi-hop networks.

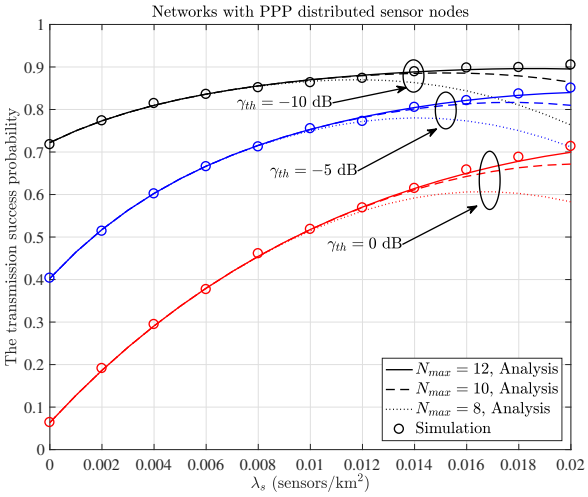

Fig. 13: Comparison of the transmission success probability for the networks with a PPP.

higher as L grows as seen in Fig. 12.

In Fig. 13, the transmission success probability $\mathcal{P}_S$ for the networks with aligned sensor nodes distributed according to a PPP is presented as a function of the intensity of sensor nodes λ_s with various values of N_{max} and γ_{th}. We mention that when the aligned sensor nodes are distributed as a PPP, the transmission success probability $\mathcal{P}_S$ is obtained by combining the approximation (62) with the expression of f_Ψ given in (52). Here, we assume $\lambda = 7$ sources/km^2, $P = -20$ dBm and $L = 300$ m. It is worthwhile to note that the derived approximated expression is well matched with the simulated results when N_{max} is set to 12. We can observe that the gaps between the approximations with small N_{max} and the simulated results increase as λ_s grows. In addition, we can see that the transmission success probability increases as λ_s grows. Although a higher λ_s increases $\mathcal{P}_T$, $\mathcal{P}_H$ is diminished as λ_s becomes larger, and therefore $\mathcal{P}_S$ is saturated as λ_s increases.

C. Star-shaped topology

In Fig. 14, we illustrate the average throughput for the networks with star-shaped topology as a function of P. We set $D \triangleq \|x_1\| = \cdots \|x_n\| = 300$ m. It is observed that when $n = 3$, our analytical results with the approximation in (67) exhibit almost identical performance with the simulation results. Note that the approximation in (67) comes from the assumption that the

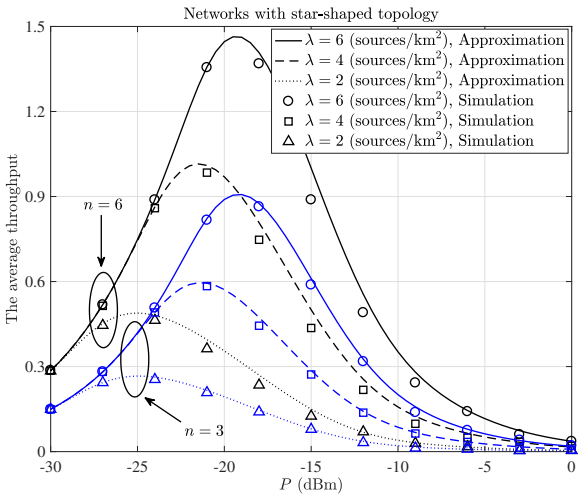

Fig. 14: Comparison of the average throughput for the networks with star-shaped topology as n varies.

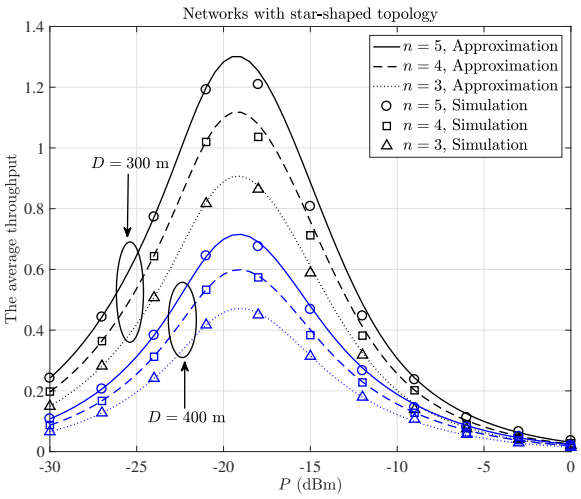

Fig. 15: Comparison of the average throughput for the networks with star-shaped topology as D varies.

events $\mathrm{A}_{\theta_k}(k > 1)$ are located in the energy harvesting enabled region are independent. If n is large, the locations of sensor nodes are more likely to be correlated, and thus, for the case of $n = 6$, there exist small gaps between the analytical results and simulation results. As expected, we can see that the average throughput becomes larger as λ increases or n grows.

Fig. 15 examines the influence of P, $D \triangleq \|x_1\| = \cdots \|x_n\|$ and n on the average throughput for the networks where $\lambda = 6$ sources/km^2. It is shown that the derived approximations well predict the performance of the networks. Note that as similar to the transmission success probability in Figs. 10 and 11, the average throughput is not a monotonic function of P since the first and second terms in the summation in (66) are an increasing and a decreasing function of P, respectively. Also, the average throughput is a monotonically increasing function of n. Moreover, we can observe that the approximation in (67) gets looser as D decreases or n increases. This is due to the fact that the probability that sensor nodes are located closely to one another increases when D is small or n is large, and this leads to a correlation among the sensor nodes.

VII. Conclusion

In this paper, we have presented a novel analytical framework based on the Boolean-Poisson model for analyzing the performance of wireless energy harvesting networks. The probability of

a single node being covered by the Boolean-Poisson model is well known. We have extended this computation to the cases of two nodes, multiple aligned nodes with fixed distances, and multiple aligned nodes distributed according to a point process. In these different settings, the performance metrics have been derived. We have also derived a tight approximation of the average throughput of networks with star-shaped topology. In addition, we have conducted an extensive simulation to validate the described analytical framework.

APPENDIX

Lemma 1. *For any $m > -1$ and $\beta > 0$, we have*

$$\int_0^\infty \frac{r^m}{r+\beta}\,\mathrm{e}^{-r}\,\mathrm{d}r = \mathrm{e}^\beta\,\mathrm{E}_{m+1}(\beta)\,\Gamma(m+1). \tag{79}$$

Proof. Starting from the right-hand side of (79), we have

$$\mathrm{e}^\beta\,\mathrm{E}_{m+1}(\beta)\,\Gamma(m+1) = \mathrm{e}^\beta \int_1^\infty \int_0^\infty u^{-m-1} v^m\,\mathrm{e}^{-(\beta u+v)}\,\mathrm{d}v\,\mathrm{d}u.$$

Then, by the bi-dimensional change of variables $u = s/(r+\beta)$ and $v = rs/(r+\beta)$, the above expression is simplified to

$$\begin{aligned}
\mathrm{e}^\beta\,\mathrm{E}_{m+1}(\beta)\,\Gamma(m+1) &= \mathrm{e}^\beta \int_0^\infty \int_{r+\beta}^\infty \Big(\frac{s}{r+\beta}\Big)^{-m-1} \Big(\frac{rs}{r+\beta}\Big)^m \mathrm{e}^{-s} \frac{s}{(r+\beta)^2}\,\mathrm{d}s\,\mathrm{d}r \\
&= \mathrm{e}^\beta \int_0^\infty \int_{r+\beta}^\infty \frac{r^m}{r+\beta}\,\mathrm{e}^{-s}\,\mathrm{d}s\,\mathrm{d}r = \mathrm{e}^\beta \int_0^\infty \frac{r^m}{r+\beta}\,\mathrm{e}^{-(r+\beta)}\,\mathrm{d}r \\
&= \int_0^\infty \frac{r^m}{r+\beta}\,\mathrm{e}^{-r}\,\mathrm{d}r,
\end{aligned}$$

which concludes the proof. □

ACKNOWLEDGEMENT

The authors would like to thank Qihao She who provided some useful insights which lead to the concise proof of Lemma 1.

REFERENCES

[1] H.-B. Kong, I. Flint, D. Niyato, and N. Privault, "On the performance of wireless energy harvesting networks in a boolean-poisson model," in *Proc. IEEE Int. Conf. on Commun. (ICC)*, pp. 1–6, May 2016.

[2] X. Lu, P. Wang, D. Niyato, D. I. Kim, and Z. Han, "Wireless networks with RF energy harvesting: A contemporary survey," *IEEE Commun. Surv. Tut.*, vol. 17, pp. 757–789, Second Quarter 2015.

[3] U. Olgun, C.-C. Chen, and J. L. Volakis, "Design of an efficient ambient WiFi energy harvesting system," *IET Microw. antennas Propag.*, vol. 6, pp. 1200–1206, Aug. 2012.

[4] M. Pinuela, P. D. Mitcheson, and S. Lucyszyn, "Ambient RF energy harvesting in urban and semi-urban environments," *IEEE Trans. Microw. Theory Techn.*, vol. 61, pp. 2715–2726, Jul. 2013.

[5] P. Nintanavongsa, M. Y. Naderi, and K. R. Chowdhury, "A dual-band wireless energy transfer protocol for heterogeneous sensor networks powered by RF energy harvesting," in *Proc. IEEE ICSEC*, Bangkok, Thailand, pp. 387-392, Sep. 2013.

[6] B. G. Karthik, S. Shivaraman, and V. Aditya, "Wi-Pie: Energy harvesting in mobile electronic devices," in *Proc. IEEE GHTC*, Seattle, WA, USA, pp. 398-401, Nov. 2011.

[7] S. N. Chiu, D. Stoyan, W. S. Kendall, and J. Mecke, *Stochastic geometry and its applications*. Third Edition, Wiley, 2013.

[8] R. Meester and R. Roy, *Continuum percolation*. Cambridge University Press, 1996.

[9] P. Hall, "On continuum percolation," *Ann. Probab.*, vol. 13, pp. 1250–1266, 1985.

[10] P. Hall, "On the coverage of k-dimensional space by k-dimensional spheres," *Ann. Probab.*, vol. 13, pp. 991–1002, 1985.

[11] H. Biermé and A. Estrade, "Covering the whole space with Poisson random balls," *ALEA Lat. Am. J. Probab. Math. Stat.*, vol. 9, pp. 213–229, 2012.

[12] J. Serra, *Image analysis and mathematical morphology*. Academic Press, 1984.

[13] F. Baccelli, Bartłomiej, and Błaszczyszyn, "On a coverage process ranging from the Boolean model to the Poisson Voronoi tessellation with applications to wireless communications," *Adv. in Appl. Probab.*, vol. 33, pp. 293–323, 2001.

[14] M. Haenggi, J. G. Andrews, F. Baccelli, O. Dousse, and M. Franceschetti, "Stochastic geometry and random graphs for the analysis and design of wireless networks," *IEEE J. Sel. Areas Commun.*, vol. 27, pp. 1029–1046, Sep. 2009.

[15] R. Zhang and C. K. Ho, "MIMO broadcasting for simultaneous wireless information and power transfer," *IEEE Trans. Wireless Commun.*, vol. 12, pp. 1989–2001, May 2013.

[16] S. Yin and Z. Qu, "Resource allocation in multiuser OFDM systems with wireless information and power transfer," *IEEE Commun. Lett.*, vol. 20, pp. 594–597, Mar. 2016.

[17] S. Timotheou, I. Krikidis, G. Zheng, and B. Ottersten, "Beamforming for MISO interference channels with QoS and RF energy transfer," *IEEE Trans. Wireless Commun.*, vol. 13, pp. 2646–2658, May 2014.

[18] H. Lee, S.-R. Lee, K.-J. Lee, H.-B. Kong, and I. Lee, "Optimal beamforming designs for wireless information and power transfer in MISO interference channels," *IEEE Trans. Wireless Commun.*, vol. 9, pp. 4810–4821, Sep. 2015.

[19] J. Park and B. Clerckx, "Joint wireless information and energy transfer in a K-user MIMO interference channel," *IEEE Trans. Wireless Commun.*, vol. 13, pp. 5781–5796, Oct. 2014.

[20] W. Huang, H. Chen, Y. Li, and B. Vucetic, "On the performance of multi-antenna wireless-powered communications with energy beamforming," *IEEE Trans. Veh. Technol.*, vol. 65, pp. 1801–1808, Mar. 2016.

[21] K. Huang and V. K. N. Lau, "Enabling wireless power transfer in cellular networks: Architecture, modeling and deployment," *IEEE Trans. Wireless Commun.*, vol. 13, pp. 902–912, Feb. 2014.

[22] J. Guo, S. Durrani, X. Zhou, and H. Yanikomeroglu, "Outage probability of ad hoc networks with wireless information and power transfer," *IEEE Wireless Commun. Lett.*, vol. 4, pp. 409–412, Aug. 2015.

[23] A. H. Sakr and E. Hossain, "Analysis of K-tier uplink cellular networks with ambient RF energy harvesting," *IEEE J. Sel. Areas Commun.*, vol. 33, pp. 2226–2238, Oct. 2015.

[24] A. H. Sakr and E. Hossain, "Cognitive and energy harvesting-based D2D communication in cellular networks: Stochastic geometry modeling and analysis," *IEEE Trans. Commun.*, vol. 63, pp. 1867–1880, May 2015.

[25] K. Huang, M. Kountouris, and V. O. K. Li, "Renewable powered cellular networks: Energy field modeling and network coverage," *IEEE Trans. Wireless Commun.*, vol. 14, pp. 4234–4247, Aug. 2015.

[26] S. Lee, R. Zhang, and K. Huang, "Opportunistic wireless energy harvesting in cognitive radio networks," *IEEE Trans. Wireless Commun.*, vol. 12, pp. 4788–4799, Sep. 2013.

[27] V. Sharma and P. Karmakar, "A novel method of opportunistic wireless energy harvesting in cognitive radio networks," in *Proc. Int. Conf. CICSyN*, pp. 59–64, Jun. 2015.

[28] M. Pratibha, K. H. Li, and K. C. Teh, "Channel selection in multichannel cognitive radio systems employing RF energy harvesting," *IEEE Trans. Veh. Technol.*, vol. 65, pp. 457–462, Jan. 2016.

[29] K. Huang, "Spatial throughput of mobile ad hoc networks powered by energy harvesting," *IEEE Trans. Inf. Theory*, vol. 59, pp. 7597–7612, Nov. 2013.

[30] Y. L. Che, L. Duan, and R. Zhang, "Spatial throughput maximization of wireless powered communication networks," *IEEE J. Sel. Areas Commun.*, vol. 33, pp. 1534–1548, Aug. 2015.

[31] B. Sklar, "Rayleigh fading channels in mobile digital communication systems part I: Characterization," *IEEE Commun. Mag.*, vol. 35, pp. 90–100, Aug. 2002.

[32] S. Li, "Concise formulas for the area and volume of a hyperspherical cap," *Asian J. Math. Stat.*, vol. 4, pp. 66–70, 2011.

[33] H. Bateman and A. Erdelyi, *Tables of Integral Transforms, Volume II*. McGraw Hill, New York, 1954.

[34] W. Yu, W. Rhee, S. Boyd, and J. M. Cioffi, "Iterative water-filling for Gaussian vector multiple-access channels," *IEEE Trans. Inf. Theory*, vol. 50, pp. 145–152, Jan. 2004.

[35] K. A. Hamdi, "A useful lemma for capacity analysis of fading interference channels," *IEEE Trans. Commun.*, vol. 58, pp. 411–416, Feb. 2010.

[36] F. Y. Kuo and I. H. Sloan, "Lifting the curse of dimensionality," *Notices AMS*, vol. 52, pp. 1320–1328, 2005.

[37] B. Blaszczyszyn and H. P. Keeler, "Studying the SINR process of the typical user in Poisson networks by using its factorial moment measures," 2014. Available: http://arxiv.org/abs/1401.4005.